Alma Mater Studiorum · Università di Bologna

Scuola di Scienze
Dipartimento di Fisica e Astronomia
Corso di Laurea Magistrale in Fisica

Primordial Black Holes in String Inflation

Relatore:
Dott. Francisco Gil Pedro

Presentata da:
Sara Zucchini

Anno Accademico 2017/2018

To my brother Lorenzo.

Abstract

In this thesis we consider the production of primordial black holes (PBH) in the context of single field inflation with the aim of describing a significant fraction of dark matter. In the models we consider, the inflaton is a string modulus and its potential is typical of type IIB fibre inflation. The potential presents a plateau at CMB scales and an extremely flat region on smaller scales. The background is analysed by solving the Friedmann's and the Klein-Gordon equations for the system. Perturbations are introduced through the usual Mukhanov-Sasaki equation for the gauge invariant curvature perturbations, whose solution allows us to find the primordial power spectrum which is then compared to observations. In the class of models considered there is an often occurring tension between the tilt of the scalar power spectrum and observations. We study this tension and propose mechanisms to minimise it. We modify the form of the fibre inflationary potential, modifying therefore the slope of the ultra slow-roll plateau. We find that a better agreement with the experimentally measured value of the spectral index can be reached. Therefore that tension between the value of the spectral index on CMB scale and the power spectrum enhancement on PBH scales can be explained as a consequence of the class of potential taken into account. This tension can be avoided in models that provide a different plateau form.

Sommario

In questa tesi considereremo la produzione di buchi neri primordiali (PBH) in un contesto di inflazione a campo singolo con lo scopo di attribuire loro una frazione significativa dell'attuale concentrazione di materia oscura. Nei modelli considerati, l'inflatone è rappresentato da un modulo il cui potenziale è tipico dell'inflazione fibrata con stringhe di tipo IIB. Il potenziale presenta un plateau nelle scale della CMB e una regione estremamente piatta su scale più piccole. Il background è analizzato risolvendo per tale sistema le equazioni di Friedmann e Klein-Gordon. Le perturbazioni vengono successivamente introdotte attraverso l'equazione di Mukhanov-Sasaki per perturbazioni di curvatura che siano gauge invarianti. Le soluzioni di tale equazione ci permettono di trovare lo spettro di potenza primordiale e compararlo alle osservazioni. I risultati trovati presentano una tensione con le osservazioni tipica della classe di modelli da noi considerata. Vengono quindi studiati e proposti meccanismi per ridurre tale disaccordo modificando la forma del potenziale inflazionario, agendo sulla pendenza del plauteau di ultra slow-roll. Si nota come in questo modo si possa ottenere un accordo migliore con le osservazioni. Dunque, la tensione fra l'indice spettrale alle scale della CMB e l'aumento nell'ampiezza dello spettro di potenza alle scale dei PBH può essere attribuita al tipo di classe di potenziali considerati. É possibile quindi evitare tale tensione utilizzando modelli che prevedono una diversa forma del plateau.

Contents

Chapter 1

A Brief Introduction to Standard Cosmology

1.1 Principles of Standard Cosmology

In this first chapter the aim is to provide an introduction to Modern Cosmology [1][2][3][4][5]. The first principle of cosmology claims that the universe is both homogeneous and isotropic on sufficiently large scales (larger than 300 million light years). Homogeneity is the property of being identical everywhere in space, while isotropy is the property of looking the same in every direction. This axiom is called the Cosmological Principle, which is consistent with observations, the prime example being the very high degree of isotropy and homogeneity of the cosmic microwave background radiation (CMB), which has a temperature of $T \sim 2.7$ K everywhere in the celestial sphere.
This principle was taken further by imposing that the universe would also look the same in all times, letting the universe be static. This takes the name of Perfect Cosmological Principle. Although the idea of a static universe did not seem plausible since the 1930s, in the 1960s, as a consequence of the first observations of CMB, models based on this principle were definitely abandoned, leaving Big Bang models as the only viable ones. As we will see later in this chapter, Big Bang models also present some problems, whose solutions requires an inflationary period. Inflation consists in a phase describing an expanding universe with positive acceleration. This mechanism is capable of solving the issues brought by the Big Bang theory and furthermore it explains how the CMB is formed and why it is homogeneous and isotropic.
Hence, the universe is expanding and its expansion is controlled by the scale factor a, in particular by its second time derivative $\ddot{a}$, whose value states an accelerated or decelerated expansion if positive or negative respectively.

A crucial parameter for the analysis of expanding universe is the Hubble parameter

$H(t)$, defined by

$$H(t) \equiv \frac{\dot{a}}{a}. \tag{1.1.1}$$

Nowadays it is known to have a value around [1]

$$H_0 \approx 65 \text{ km s}^{-1} \text{ Mpc}^{-1}. \tag{1.1.2}$$

Through its value it is possible to have an estimate of the age of the universe as

$$t_0 < \frac{1}{H_0} \sim 13 \cdot 10^9 \text{ years}, \tag{1.1.3}$$

where $1/H_0$ is the Hubble time.

Theories of Cosmology are based on Einstein's General Relativity [1][6][7] and are described by Einstein equations

$$G_{\mu\nu} \equiv R_{\mu\nu} - \frac{1}{2} g_{\mu\nu} R = \frac{8\pi G}{c^2} T_{\mu\nu}, \tag{1.1.4}$$

where $R_{\mu\nu}$ is the Ricci tensor, $R = R^{\mu}_{\mu} = g^{\mu\nu} R_{\mu\nu}$ the Ricci scalar, $T_{\mu\nu}$ the energy-momentum tensor and G the gravitational constant. $G_{\mu\nu}$ is the so called Einstein's tensor. Later a second form of this equation was proposed

$$R_{\mu\nu} - \frac{1}{2} g_{\mu\nu} R - \Lambda g_{\mu\nu} = \frac{8\pi G}{c^2} T_{\mu\nu}, \tag{1.1.5}$$

where a term containing the cosmological constant Λ is added.
When it was initially proposed, Λ was supposed to be interpreted as adding term to the geometry of the universe, in order for Einstein to obtain an equation describing a static ($\dot{a} = 0$) universe, since it was the generally accepted view by cosmologists of the time and from (1.1.4) he could only obtain non-static solutions.
For an empty universe we have a Minkowski space $R_{\mu\nu} - \frac{1}{2} g_{\mu\nu} R = 0$ from (1.1.4), while from (1.1.5) we have solutions that describe a curved geometry $R_{\mu\nu} - \frac{1}{2} g_{\mu\nu} R + \Lambda g_{\mu\nu} = 0$, even if no matter is present. Universes of this type have a constant scalar curvature $R = const$ and are called de Sitter universes if $\Lambda > 0$ and anti-de Sitter if $\Lambda < 0$. These special solutions, in particular the de Sitter one, are interesting in a cosmological context, both in the early and late universe.

Considering also the contribution of Λ, the components forming the universe are essentially three: the Λ component, which is associated with dark energy, the radiation and matter's components, whose contribution are baryonic and dark matter.

Theories containing dark matter arise as natural consequence from observations on galaxies' masses and their velocity, noticing that a new type of non-luminous matter is present. It is not directly observable, since it only interacts gravitationally, and its nature has remained a mystery.
Different properties can be searched for in the description of particles composing dark matter: hot dark matter (HDM), whose components are relativistic particles, or cold dark matter (CDM), whose components are non-relativistic.
In the past two decades observations (most recently the observations of the Planck satellite) have established a standard model of cosmology, the ΛCDM model, which requires a universe described by the Einstein equations (1.1.5) and dark matter of cold type. From observations we can state that our universe is filled with 68% dark energy, 27% dark matter, and only 5% baryonic matter [8].

In this thesis we will investigate the connection between the dark matter problem and cosmic inflation. We study the possibility that dark matter is formed by very light, atomic sized primordial black holes produced by density perturbations generated during inflation. Our main aim will be to render the primordial black holes production mechanism compatible with CMB constraints on the curvature power spectrum.

1.1.1 FRW Spacetime

This sort of spacetime is described by the Friedmann-Robertson-Walker (FRW) metric:

$$\mathrm{d}s^2 = -c^2\mathrm{d}t^2 + a^2(t)\left[\frac{\mathrm{d}r^2}{(1-kr^2)} + r^2\mathrm{d}\Omega^2\right], \tag{1.1.6}$$

where k gives the curvature of the space-like 3-hypersurface: $k = 0$ describes a flat 3D-space, while $k = +1$ and $k = -1$ describe a positively and negatively curved surface respectively.
In order to simplify the notation, we will stick to the case $k = 0$ and define the conformal time

$$\mathrm{d}\tau = \frac{\mathrm{d}t}{a(t)}. \tag{1.1.7}$$

As a consequence, the FRW metric in (1.1.6) can be written as

$$\mathrm{d}s^2 = a^2(\tau)[-\mathrm{d}\tau^2 + \mathrm{d}r^2 + r^2\mathrm{d}\Omega^2] = a^2(\tau)\eta_{\mu\nu}dx^\mu dx^\nu \tag{1.1.8}$$

and factorized into a Minkowski metric $\eta_{\mu\nu}$ multiplied by the scale factor $a(\tau)$.

The radial propagation of photons is described by a 2-dimensional metric

$$\mathrm{d}s^2 = a^2(\tau)[-\mathrm{d}\tau^2 + \mathrm{d}r^2] \tag{1.1.9}$$

and the maximal distance they can cover is given by

$$\Delta r = \Delta\tau \equiv \tau - \tau_i = \int_{t_i}^{t} \frac{\mathrm{d}t'}{a(t')}, \tag{1.1.10}$$

where $t > t_i$ and t_i is the initial time. If $t_i = 0$ is taken to be the initial time of the universe where a singularity occurs for $a_i = a(t_i = 0) = 0$

$$\Delta r = \int_{0}^{t} \frac{\mathrm{d}t'}{a(t')} = \tau(t) - \tau(0). \tag{1.1.11}$$

Δr is called the comoving horizon.

1.1.2 Friedmann's Models and the Inevitability of the Big Bang

Considering the homogeneity and the isotropy of the universe, it can be treated as a perfect fluid

$$p = w\rho c^2, \tag{1.1.12}$$

where $0 \leq w < 1$ is the Zeldovich interval. Thus the energy-momentum tensor T_{ij} becomes

$$T_{ij} = (p + \rho c^2)U_i U_j - p g_{ij}, \tag{1.1.13}$$

where U_k is the fluid 4-velocity. The Einstein's equation and the perfect fluid approximation yield together the Friedmann's equations

$$\ddot{a} = -\frac{4\pi}{3} G \left(\rho + 3\frac{p}{c^2}\right) a \tag{1.1.14}$$

$$a\ddot{a} + 2\dot{a} + 2kc^2 = 4\pi G \left(\rho - \frac{p}{c^2}\right) a, \tag{1.1.15}$$

for the time-time and space-space component respectively.
Using the first Friedmann's equation, the second simplifies to

$$\dot{a}^2 + kc^2 = \frac{8\pi G}{3}\rho a^2. \tag{1.1.16}$$

In case of models that include the cosmological constant, these equations become

$$\ddot{a} = -\frac{4\pi}{3} G \left(\tilde{\rho} + 3\frac{\tilde{p}}{c^2}\right) a \tag{1.1.17}$$

$$\dot{a}^2 + kc^2 = \frac{8\pi G}{3}\tilde{\rho} a^2, \tag{1.1.18}$$

where $\tilde{\rho} = \rho + \frac{\Lambda c^2}{8\pi\ G}$ and $\tilde{p} = p - \frac{\Lambda c^4}{8\pi\ G}$ are the effective mass density and pressure.

The two equations (1.1.14) and (1.1.16) are not independent, but instead they are bounded through the adiabatic relationship

$$\mathrm{d}U = -p\mathrm{d}V, \tag{1.1.19}$$

which becomes

$$\mathrm{d}\big(c^2\rho a^3\big) = -p\mathrm{d}a^3. \tag{1.1.20}$$

Models based on the perfect fluid approximation are called Friedmann's models and for these we can study the evolution of the different densities composing the universe using both (1.1.12) and (1.1.20)

$$\begin{aligned} \mathrm{d}\big(\rho c^2 a^3\big) &= -w\rho c^2 \mathrm{d}a^3 \\ \mathrm{d}\rho a^3 + \mathrm{d}a^3\rho &= -w\rho\mathrm{d}a^3 \\ \mathrm{d}\rho a^3 &= -\rho\mathrm{d}a^3(1+w) \\ \frac{\mathrm{d}\rho}{\rho} &= -\frac{\mathrm{d}a^3}{a^3}(1+w), \end{aligned} \tag{1.1.21}$$

which gives the behaviour of ρ depending on w

$$\rho \propto a^{-3(1+w)}. \tag{1.1.22}$$

Once it is normalized, we obtain $\rho_{mat} = \rho_{mat0}\left(\frac{a}{a_0}\right)^{-3}$ since for matter $w = 0$, while for radiation $w = 1/3$ and $\rho_{rad} = \rho_{rad0}\left(\frac{a}{a_0}\right)^{-4}$.

As we already noticed, another factor has to be considered and it is the one brought by the cosmological constant Λ, introduced in the Einstein's equations (1.1.4) by Einstein himself as adding term to the spacetime side of this equation

$$R_{ij} - \frac{1}{2}g_{ij}R - \Lambda g_{ij} = \frac{8\pi G}{c^4}T_{ij}. \tag{1.1.23}$$

For this type of contribution $w = -1$, therefore its density is constant in time

$$\rho_\Lambda = \rho_{\Lambda 0}. \tag{1.1.24}$$

An important parameter is the density parameter, which is detectable and can give us information about the ρ of different components. We can define it as

$$\Omega = \frac{\rho}{\rho_{crit}}, \tag{1.1.25}$$

where $\rho_{crit} = 3H^2/8\pi G$ and its value today is $\rho_{crit0} = 3H_0^2/8\pi G \approx 2.78\ 10^{11} h^2 M_\odot/\text{Mpc}$, where h is defined as $h = H_0/(100\ \text{km s}^{-1}\ \text{Mpc}^{-1})$. The values the density parameters assume today for matter, radiation and cosmological constant are the following respectively: $\Omega_{mat0} \approx 0.3$, $\Omega_{rad0} \approx 10^{-5}$ and $\Omega_{\Lambda 0} \approx 0.7$.

Substituting (1.1.12) in (1.1.14), we have

$$\ddot{a} = -\frac{4\pi}{3} G\rho(1+3w)a \tag{1.1.26}$$

and we can point out that, if for ordinary matter the Zeldovich interval is valid, the term $(1+3w)$ must always be positive and for this reason $\ddot{a}$ is negative, meaning that for a Friedmann's universe a decelerated expansion is expected.
Since $\ddot{a} < 0$ and $\dot{a} > 0$, then there must be a singularity at a finite time in the past, i.e. a point when $a = 0$.

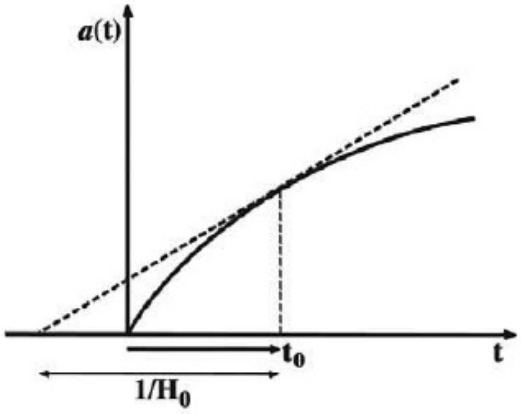

Figure 1.1: Plot of $a(t)$. If $\dot{a}(t) > 0$ and $\ddot{a}(t) < 0$, $a(t)$ must be 0 at some point in the past: the Big Bang. Source [1].

This moment is called the Big Bang singularity and it also ensures that the age of the universe t_0 is smaller than the Hubble time $1/H_0$, as seen in (1.1.3) and in Figure 1.1.

Considering the Big Bang singularity as intial point for our universe, the first period we can get information about through observations is the Planck era, starting from $t_p \simeq 10^{-43}$ s. To this time is related a temperature $T_p \simeq 10^{19}$ GeV. Between T_p and $200 - 300$ MeV three phase transitions can be identified.
Before t_p no information can be obtained, since quantum cosmology is necessary.

The first phase transition we consider is the Grand Unification Theory transition, whose

name has to be referred to the fact that, before this transition, all the forces were united. In fact, this is the period were the strong and the electro-weak forces separate each others, creating leptons and hadrons as distinct particles.
To this era is associated a time $t_{GUT} \simeq 10^{-37}$ s and a temperature $T_{GUT} \simeq 10^{15}$ GeV. Inflation takes place in the time between the Planck era and the GUT transition.

The next occurring phase transition is the Electro-Weak ($t_{EW} \simeq 10^{-11}$ s and $T_{EW} \simeq 10^2$ GeV), where the electromagnetic and the weak forces separate.

The last phase transition is the Quark-Hadron ($t_{QH} \simeq 10^{-5}$ s and $T_{QH} \simeq 200-300$ MeV), which leads to the confinement of quarks into hadrons.

1.2 The need for Inflation

In this section we will study some problems that the Big Bang theory presents, such as the horizon problem, the flatness (or age) problem and the exotic particles problem. Around 1980 a mechanism able to solve these problems was proposed: it consists in the introduction of a period, called inflation, where the universe is expanding with a positive acceleration. Besides solving the issues brought by the Big Bang theory, it is also capable to explain how the cosmological principle of homogeneity and isotropy arises, allowing us to avoid taking it as an axiom but providing us a dynamical explanation instead.

1.2.1 The Horizon Problem

This problem arises from the difference in values between the cosmological horizon R_H and the last scattering surface R_{ls} [1].
The former is the finite region containing the points in causal connection while the latter is the surface described at the moment the CMB is generated, which corresponds to the last scattering between radiation and matter. At τ_{rec} the scattering rate between matter and photons becomes negligible, yielding the radiation-matter decoupling and providing the photons with an infinite mean free path, constituting afterwards to the CMB. As we already pointed out in section 1.1, from observations the CMB is observed to be homogeneous and isotropic (in a range of temperature about one part on 10^5). This suggests that the last scattering must be occurred in thermal equilibrium, i.e. must be generated within the region inside the cosmological horizon.
Despite this fact, if we evaluate R_{ls}, it happens to be larger than the horizon R_H calculated at the same time z_{ls}, therefore according to Big Bang cosmology the CMB was created in a region outside the horizon, which means that some of its points were never in causal contact. Another way to explain this is that the conformal time between the Big Bang singularity and the decoupling of the CMB from the matter is not enough to

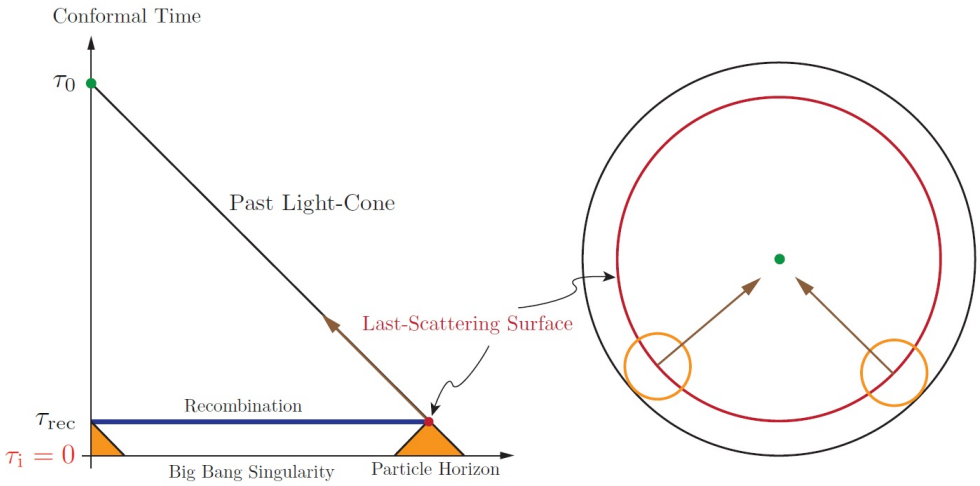

Figure 1.2: The diagram shows no causal contact in most spots of the CMB for a standard FRW cosmology. The Big Bang singularity is thought to take place at $\tau = 0$. After this time, at finite τ_{rec} the decoupling between matter and radiation occurs, originating in this way the CMB. Source [9].

have overlapping past light cones [9][10], see Figure 1.2, that again leads to a lack of causal contact among different points of the CMB, although we can observe it.

A simple solution to this problem is the introduction of a phase called inflation where the universe expands with a positive acceleration $\ddot{a} > 0$.

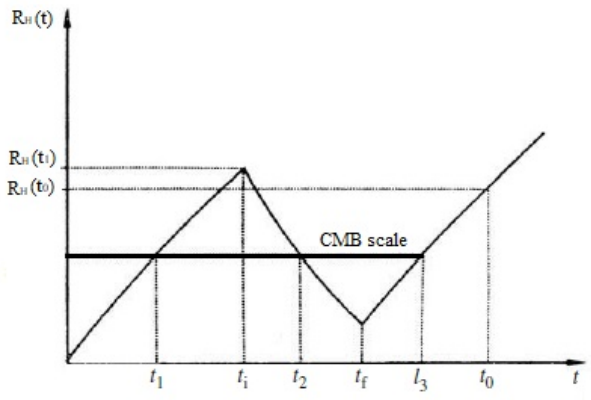

Figure 1.3: Thanks to inflation, the CMB scale enters the horizon at t_1 and leaves at t_2, then re-enters at t_3. Source [1].

In this way, we can state that the CMB scale enters the horizon at t_1, leaves during inflation at t_2 and re-enters at t_3. This means that the CMB was created within the horizon region, leading to overlapping light cones, i.e. causal contact among all points in the sky.

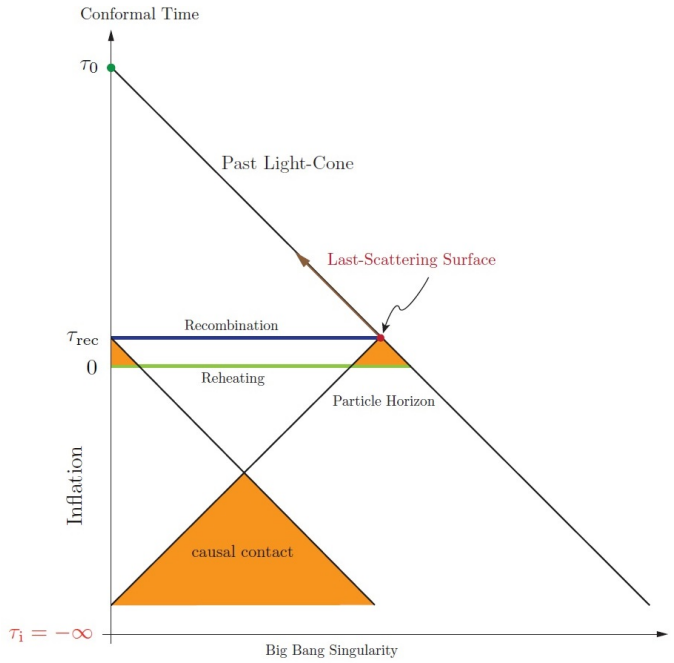

Figure 1.4: Conformal time diagram for inflationary cosmology. The Big Bang singularity occurs at $\tau = -\infty$. After this, for a finite $\tau < 0$ an inflationary period takes place ending at $\tau = 0$ with the reheating phase. At τ_{rec} the decoupling between matter and radiation occurs, originating in this way the CMB. Source [9].

In terms of the conformal time, during inflation the Hubble radius is decreasing

$$\frac{d}{dt}(aH)^{-1} < 0. \tag{1.2.1}$$

If this condition lasts long enough, the horizon would shrink such that the horizon problem can be avoided.
The solution is to push the Big Bang singularity to a negative conformal time, leading in this way to a larger time interval between the Big Bang and the CMB formation

$$\tau_i \propto \frac{2}{(1+3w)} a_i^{\frac{1}{2}(1+3w)}, \tag{1.2.2}$$

where $w < -1/3$ during inflation, therefore the Big Bang singularity is shifted to $\tau_i = -\infty$.

Now the initial time is no longer considered to be at $\tau = 0$ but at $\tau = -\infty$ and $\tau = 0$ becomes the time inflation ends, entering the reheating phase and starting the baryogenesis, see Figure 1.4.

1.2.2 The Flatness Problem

Another problem arising from the Big Bang model is the flatness problem [9][1].
As already seen, considering the second Friedmann's equation with a spatial curvature, i.e. $k \neq 0$, and simplifying it using (1.1.14), we obtain

$$\dot{a}^2 + kc^2 = \frac{8\pi}{3} G\rho a^2.$$

We can now express it in terms of the Hubble parameter and then of the density parameter, with c=1

$$\begin{aligned} H^2 &= -\frac{k}{a^2} + \frac{8\pi}{3}\rho \\ 1 - \Omega(a) &= -\frac{k}{(aH)^2}. \end{aligned} \tag{1.2.3}$$

From (1.2.3) we can state that if the universe is flat, it tends to remain flat for all time, since $k = 0$ would lead to $\Omega(a) = const(= 1)$ for every a, which in terms of time becomes $\Omega(t) = const$. On the other hand, if the universe carries some curvature at early times, it will grow.
From observations we know that today $|1 - \Omega(a_0)| \lesssim 0.01$, hence Ω is today close to 1. From (1.2.3) it is clear that $|1 - \Omega(a)|$ is a function of $(aH)^{-1}$, which in standard conditions tends to increase in time, making the curvature grow. In early times the flatness was more extreme, for instance in the GUT epoch $|1 - \Omega(a_{GUT})| \lesssim 10^{-55}$.

We can refer to this problem also as the age problem: if the universe presented a positive curvature (closed universe), it would have rapidly recollapsed near the Planck time t_p, while if it presented a negative curvature (open universe), the curvature term k^2c^2/a^2 in the Friedmann's equation (1.1.16) would have dominated causing to reach the present temperature in $t_0 \approx 10^{-11}$ s, which would be the age of the universe today. From the Hubble parameter we can evaluate t_0 and state that the only consistent case we can obtain is a universe described by $k = 0$.

The flatness problem states that such finely tuned initial conditions seem extremely unlikely. Any other initial condition different from $\Omega = 1$ at early times would have led to a curved universe at present time, with a value of Ω much far from 1, see Figure 1.5.

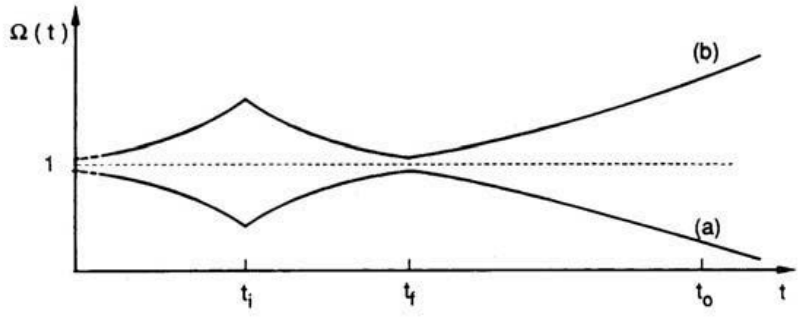

Figure 1.5: Evolution of $\Omega(t)$ for an open (a) and a closed universe (b). Inflation occurs in the time interval (t_i, t_f), yielding an accelerated expansion and driving $\Omega(t_f)$ close to 1. Source [1].

The solution for this problem can be found by introducing an inflationary period: in this phase we require that the Hubble sphere is decreasing and for this reason inflation drives the universe to unity of Ω, leading to a flat universe with a present age of $t_0 \sim 10^{10}$ s.

1.2.3 Exotic Particles Problem

Exotic particles are produced in the early universe in phase transition and symmetry breaking processes. These particles are also called cosmic relics and they have not been detected today even tough they should have been copiously produced in the early universe. The solution to this problem, as we will see later in this section, will be the introduction of an inflationary period which will dilute those kind of particles away.

Two types of exotic particles can be created. The first is constituted by thermal relics, which are produced and remain in thermal equilibrium with other components of the universe until decoupling, like the massless neutrino. This class can be further divided in hot and cold relics, where the former are relativistic at the decoupling time, while the latter are not. The second type of exotic particles are the non-thermal relics, that are not produced in thermal equilibrium, like axions and magnetic monopoles.

As example of these exotic particles we can study the magnetic monopoles. It is possible to estimate the mass and the abundance [1] they are expected to carry at the GUT time t_{GUT}:

$$m_{MM} \sim 10^{16}\text{GeV} \tag{1.2.4}$$

$$n_{MM} > 10^{-10} n_\gamma \tag{1.2.5}$$

where n_γ is the abundance of photons at t_{GUT}.
Since the ratio n_{MM}/n_γ remains constant in time and today the number of photons is 10^{10} larger than the one of baryons, we can state that the number of monopoles today should approximately be the number of baryons today $n_{MM0} \simeq n_{bar0}$. It means that nowadays we should observe as many monopoles as baryons, but this does not happen.

Furthermore, the density parameter for monopoles is $\Omega_{MM} > (m_{MM}/m_{bar})\ \Omega_{bar} \simeq 10^{16}$, which seems absurdly large and would cause an almost instant closure of the universe.

Once again, the solution is to introduce an inflationary period, where the universe is subjected to such an expansion that the monopole are diluted, leaving less than one monopole per present horizon scale. In this way their concentration is reduced and their density parameter becomes smaller. We decided to display the monopoles problem, but this analysis can be extended to all types of exotic particles and for them the solution is also to introduce a period with accelerated expansion.

Chapter 2

The Physics of Inflation

2.1 Conditions for Inflation

As we already stated in the previous chapter, the main condition for inflation [9] is the **shrinking Hubble sphere**

$$\frac{d}{dt}(aH)^{-1} < 0,$$

but this definition leads to other equivalent ways of describing inflation.

For instance another way to write it, introducing a relation we already introduced in section 1.2.1, can be $\ddot{a} > 0$. Let us see where it comes from:

$$\frac{d}{dt}(aH)^{-1} = \frac{d}{dt}(\dot{a})^{-1} = -\frac{\ddot{a}}{\dot{a}^2} \tag{2.1.1}$$

since the Hubble sphere must decrease, we expect an **accelerated expansion**

$$\frac{d^2a}{dt^2} > 0. \tag{2.1.2}$$

The shrinking Hubble sphere can also be used to define some parameters that control inflation

$$\frac{d}{dt}(aH)^{-1} = -\frac{\dot{a}H + a\dot{H}}{(aH)^2} = -\frac{1}{a}(1-\varepsilon) \tag{2.1.3}$$

where $\varepsilon \equiv -\dot{H}/H^2$ is always a positive quantity. Another bound on ε can be set using the shrinking Hubble sphere condition defining the number of e-folds N of inflationary expansion $\mathrm{d}N \equiv \mathrm{d}\ln a = H\mathrm{d}t$

$$\varepsilon = -\frac{\dot{H}}{H^2} \tag{2.1.4}$$

$$= -\frac{d\ \ln H}{dN} < 1. \tag{2.1.5}$$

It implies that the Hubble parameter per number of e-fold changes slowly and inflation ends once ε reached 1. We can yet state that an additional condition to inflation is that the **Hubble parameter** must be **nearly constant**.

Another important factor has to be considered: inflation must last long enough (from 40 to 60 e-folds) to solve the above cosmological problems brought by the Big Bang model. To measure that ε actually remains small for sufficiently long time, we introduce

$$\eta = \frac{\dot{\varepsilon}}{H\varepsilon} \tag{2.1.6}$$

$$= \frac{d\ \ln\varepsilon}{dN}. \tag{2.1.7}$$

As long as $|\eta| < 1$ inflation persists.

In the de Sitter limit $\varepsilon \to 0$ and the space grows exponentially in time as $a(t) \propto e^{Ht}$, where $H \approx const.$ We have already seen that in Friedmann's models the perfect fluid approximation (1.1.12) is valid. Substituting it in the Friedmann's equation (1.1.14), we obtain

$$\dot{H} + H^2 = -\frac{4\pi}{3}G(\rho + 3p) = -\frac{H^2}{2}\left(1 + \frac{3p}{\rho}\right)$$

$$\dot{H} = -\frac{3H^2}{2}\left(1 + \frac{p}{\rho}\right) \tag{2.1.8}$$

This yields

$$\varepsilon = -\frac{\dot{H}}{H^2} = \frac{3}{2}\left(1 + \frac{p}{\rho}\right) < 1$$

where w is defined as $w \equiv p/\rho$ and $w < -1/3$ during the inflationary phase, as we have already seen in section 1.2.1.
It means that inflation requires a **negative pressure**.

2.2 Background evolution

Let us consider a background FRW space-time, a spatially homogeneous scalar field ϕ with Lagrangian density

$$\mathcal{L}(\phi) = 1/2\ \partial^\mu\phi\partial_\mu\phi - V(\phi) = \dot{\phi}^2/2 - V(\phi). \tag{2.2.1}$$

The stress-energy tensor for this field is $T^{\mu\nu} = \partial^\mu\phi\partial_\mu\phi - \mathcal{L}(\phi)g^{\mu\nu}$. Since ϕ is homogeneous, $T^{\mu\nu}$ takes the form of a perfect fluid with effective energy density and effective pressure

$$\rho_\phi = \dot{\phi}^2/2 + V(\phi) \tag{2.2.2}$$

$$p_\phi = \dot{\phi}^2/2 - V(\phi) \tag{2.2.3}$$

By using the Eulero-Lagrange equation

$$\frac{\mathrm{d}}{\mathrm{d}t}\frac{\partial}{\partial\dot{\phi}}L - \frac{\partial}{\partial\phi}L = 0 \tag{2.2.4}$$

where $L = \mathcal{L}a^3$ is the Lagrangian, we can find the equation of motion for ϕ

$$\ddot{\phi} + 3H\dot{\phi} + \frac{\partial}{\partial\phi}(V) = 0. \tag{2.2.5}$$

In order to be sure that the inflationary period lasts long enough to solve the horizon problem, it is useful to impose some conditions, called slow roll conditions:

$$\dot{\phi}^2 \ll V(\phi) \tag{2.2.6}$$

$$\ddot{\phi} \approx 0\ . \tag{2.2.7}$$

The (2.2.6) let the kinetic term be negligible requiring a flat potential, while the (2.2.7) describes a non-accelerated field.

Consider the second Friedmann's equation (1.1.16) rewritten in terms of H and as a function of the reduced Planck mass $M_p^{-2} \equiv 8\pi G = (2.4\ 10^{18} GeV)^{-2}$ (usually set to one)

$$H^2 = \frac{1}{3M_p^2}\left(\frac{\dot{\phi}^2}{2} + V(\phi)\right). \tag{2.2.8}$$

It is possible to evaluate ε and η from 2.1.4 and 2.1.6 and to do that it is useful to derive the continuity equation from equations (2.2.5) and (2.2.8)

$$\dot{H} = -\frac{1}{2}\frac{\dot{\phi}^2}{M_p^2}. \tag{2.2.9}$$

Now ε can be written as

$$\varepsilon = \frac{1/2\ \dot{\phi}^2}{H^2 M_p^2}. \tag{2.2.10}$$

The first slow roll condition (2.2.6) implies

$$H^2 \simeq \frac{V}{3M_p^2} \tag{2.2.11}$$

and, using the second slow roll condition (2.2.7), the equation of motion (2.2.5) becomes

$$3H\dot{\phi} \simeq -V_\phi \tag{2.2.12}$$

hence ε can be written as

$$\varepsilon(\phi) \simeq \frac{M_p^2}{2}\left(\frac{V_\phi}{V}\right)^2. \tag{2.2.13}$$

In the same way

$$\eta(\phi) \simeq M_p^2\left(\frac{V_{\phi\phi}}{V}\right) \tag{2.2.14}$$

where V_ϕ and $V_{\phi\phi}$ are the first and the second derivatives of the potential V taken with respect to ϕ.

Using the equation of motion (2.2.5) and the (2.2.11), we can see that

$$\left|\frac{V_{\phi\phi}}{V}\right| \ll 1 \tag{2.2.15}$$

$$\left|\frac{V_\phi}{V}\right|^2 \ll 1, \tag{2.2.16}$$

thus, as already seen in section 2.1, ε and η, taking respectively the form (2.2.13) and (2.2.14), must both be $\ll 1$ to permit inflation to occur.

Another important value we have introduced is the number of e-folds, which can be used to measure the duration of inflation. Using the definition of N

$$N \equiv \int_{a_i}^{a_m} \mathrm{d}\ln a = \int_{tf}^{ti} H(t)\mathrm{d}t, \tag{2.2.17}$$

the approximations both of H in (2.2.11) and of the equation of motion in (2.2.12), we can obtain the behaviour of N in terms of the field ϕ

$$\begin{aligned} H\mathrm{d}t = \frac{H}{\dot\phi}\mathrm{d}\phi = -\frac{H}{V_\phi/3H}\mathrm{d}\phi = -\frac{3H^2}{V_\phi} \\ = -\frac{3H^2}{\sqrt{2\varepsilon}V}M_p\mathrm{d}\phi = -\frac{1}{\sqrt{2\varepsilon}M_p}\mathrm{d}\phi \\ \Rightarrow N = \int_{\phi_i}^{\phi_f}\frac{1}{\sqrt{2\varepsilon}M_p}\mathrm{d}\phi \end{aligned} \tag{2.2.18}$$

where ϕ_i and ϕ_f are defined as the boundaries of the interval where $\varepsilon < 1$.
As already stated in section 2.1, the e-folds number must be $N \simeq 40 - 60$ to obtain a successful solution to the horizon problem.

2.3 Cosmological perturbation theory

In this section primordial perturbation are studied. By introducing them the variation of 1 part on 10^5 in the CMB temperature can be explained.

2.3.1 Classical Perturbations

Consider a single-field slow roll model of inflation, whose action can be written as

$$S = \int \mathrm{d}^4x\sqrt{-g}\left[\frac{1}{2}\mathcal{R} - \frac{1}{2}g^{\mu\nu}\partial_\mu\phi\partial_\nu\phi - V(\phi)\right], \tag{2.3.1}$$

where $\mathcal{R}$ is the 4-dimensional Ricci scalar and $\sqrt{-g}$ is the determinant of the metric $g_{\mu\nu}$. We have four metric perturbations δg_{00} , δg_{ii}, δg_{0i} and δg_{ij} and one scalar perturbation $\delta\phi$. Two are removed by the Einstein constraint equation and other two from the invariance of the action under the coordinate transformation $t \to t + \epsilon_0, x_i \to x_i + \partial_i\epsilon$, letting the physical mode be just one.

It is convenient to work in a fixed gauge where the momentum density is vanishing $\delta T_{0i} \equiv 0$, which becomes $\delta\phi = 0$ in the slow roll inflation. In this gauge, perturbations are characterized purely by fluctuations in the metric

$$\delta g_{ij} = a^2(1 - 2\zeta)\delta_{ij} + a^2 h_{ij}, \tag{2.3.2}$$

where the perturbations are carried by the term $-a^2\zeta\delta_{ij}$. h_{ij} is a transverse traceless tensor and ζ is a scalar and it is time-independent on the super-horizon scale $k \ll aH$

$$\lim_{k\ll aH}\dot{\zeta}_k = 0. \tag{2.3.3}$$

By substituting (2.3.2) for the components $(0,0)$ and $(0,i)$ in the action (2.3.1) and expanding in powers of ζ, we find

$$S = \frac{1}{2}\int \mathrm{d}t\ \mathrm{d}^3\mathbf{x}\ a^3\frac{\dot{\phi}^2}{H^2}\left[\dot{\zeta}^2 - \frac{1}{a^2}(\partial_i\zeta)^2\right] + ... \tag{2.3.4}$$

Let us define

$$v \equiv z\zeta \tag{2.3.5}$$

the canonically normalized Mukhanov variable, where

$$z^2 \equiv a^2\frac{\dot{\phi}^2}{H^2} = 2a^2\varepsilon. \tag{2.3.6}$$

We can now express the action in conformal time τ

$$S = \frac{1}{2}\int \mathrm{d}\tau\ \mathrm{d}^3\mathbf{x}\left[(v')^2 - (\partial_i v)^2 + \frac{z''}{z}v^2\right] \tag{2.3.7}$$

and recognize the harmonic oscillator action with the effective mass equal to

$$m^2_{eff}(\tau) \equiv -\frac{z''}{z}, \tag{2.3.8}$$

which is time-dependent.

From (2.3.7), we obtain the Mukhanov-Sasaki equation

$$v_{\mathbf{k}}^2 + \left(k^2 - \frac{z''}{z}\right) v_{\mathbf{k}} = 0, \tag{2.3.9}$$

where we defined the Fourier modes

$$v_{\mathbf{k}} \equiv \int \mathrm{d}^3\mathbf{x}\; e^{-i\mathbf{k}\cdot\mathbf{x}} v(\tau, \mathbf{x}) \tag{2.3.10}$$

and where the term $(k^2 - z''/z)$ represents the effective frequency $\omega_k^2(\tau)$ of the modes $v_{\mathbf{k}}$.

Its most general solution, since the frequency $\omega_k(\tau)$ depends only on $k \equiv |k|$, is given by the expansion of the complex modes $v_k(\tau)$ and $v_k^*(\tau)$:

$$v_{\mathbf{k}} \equiv a_{\mathbf{k}}^- v_k(\tau) + a_{\text{-}\mathbf{k}}^+ v_k^*(\tau), \tag{2.3.11}$$

where $a_{\mathbf{k}}^-$ and $a_{\text{-}\mathbf{k}}^+$ are two time-independent complex constant. The Wronskian of the functions $v_k(\tau)$ and $v_k^*(\tau)$ is defined as

$$W[v_k, v_k^*] \equiv v_k' v_k^* - v_k v_k'^* = 2iIm(v_k' v_k^*) \tag{2.3.12}$$

and always satisfies, through a rescaling of the mode functions as $v_k \to \lambda v_k \Rightarrow W[v_k, v_k^*] \to |\lambda|^2 W[v_k, v_k^*]$, the normalization

$$W[v_k, v_k^*] \equiv -i. \tag{2.3.13}$$

Through the Fourier transforming of the solution in (2.3.11), we have

$$v(\tau, \mathbf{x}) = \int \frac{\mathrm{d}^3\mathbf{k}}{(2\pi)^{3/2}} [a_{\mathbf{k}}^- v_k(\tau) e^{i\mathbf{k}\cdot\mathbf{x}} + a_{\text{-}\mathbf{k}}^+ v_k^*(\tau) e^{-i\mathbf{k}\cdot\mathbf{x}}]. \tag{2.3.14}$$

2.3.2 Quantum origin of Perturbations

To obtain the quantisation we promote to operators the field v ad its momentum $\pi \equiv v'$, which satisfy the equal-time commutation relations

$$[\hat{v}(\tau, \mathbf{k}), \hat{\pi}(\tau, \mathbf{y})] = \delta(\mathbf{x} - \mathbf{y}) \tag{2.3.15}$$

$$[\hat{v}(\tau, \mathbf{k}), \hat{v}(\tau, \mathbf{y})] = [\hat{\pi}(\tau, \mathbf{k}), \hat{\pi}(\tau, \mathbf{y})] = 0. \tag{2.3.16}$$

In the same way, the standard commutation rules are valid for the complex constant

$a^-_{\mathbf{k}}$ and $a^+_{\mathbf{-k}} = (a^-_{\mathbf{k}})^*$ once we operated the canonical quantization turning them into the operators $\hat{a}^-_{\mathbf{k}}$ and $\hat{a}^+_{\mathbf{k}}$.

$$[\hat{a}^-_{\mathbf{k}}, \hat{a}^+_{\mathbf{k'}}] = \delta(\mathbf{k} - \mathbf{k'}) \tag{2.3.17}$$
$$[\hat{a}^-_{\mathbf{k}}, \hat{a}^-_{\mathbf{k}}] = [\hat{a}^+_{\mathbf{k}}, \hat{a}^+_{\mathbf{k'}}] = 0. \tag{2.3.18}$$

Hence the solution (2.3.14) becomes:

$$\hat{v}(\tau, \mathbf{x}) = \int \frac{\mathrm{d}^3\mathbf{k}}{(2\pi)^{3/2}} [\hat{a}^-_{\mathbf{k}} v_k(\tau) e^{i\mathbf{k}\cdot\mathbf{x}} + \hat{a}^+_{\mathbf{k}} v^*_k(\tau) e^{-i\mathbf{k}\cdot\mathbf{x}}]. \tag{2.3.19}$$

The operators $\hat{a}^-_{\mathbf{k}}$ and $\hat{a}^+_{\mathbf{k}}$ can be interpreted as the annihilation and creation operators and used together with the vacuum state $|0\rangle$ to create quantum states in the Hilbert space

$$\hat{a}^-_{\mathbf{k}} |0\rangle = 0, \quad \hat{a}^+_{\mathbf{k}} |0\rangle = |1_{\mathbf{k}}\rangle . \tag{2.3.20}$$

To create further excited states we will use

$$|m_{\mathbf{k}}, n_{\mathbf{p}}, ...\rangle = \frac{1}{\sqrt{m!n!...}} \left[(\hat{a}^+_{\mathbf{k}})^m (\hat{a}^+_{\mathbf{p}})^n ...\right] |0\rangle , \tag{2.3.21}$$

where $(k, p, ...)$ are the particles' momenta.

In the physical interpretation of the quantum states ambiguity arises, since the vacuum we may choose can not be interpreted as unique. Let us consider the functions

$$u_k(\tau) = \alpha_k v_k(\tau) + \beta_k v^*_k(\tau), \tag{2.3.22}$$

where α_k and β_k are complex constant. We will prove later in this section that, introducing some conditions, these functions can be seen as modes of the Mukhanov-Sasaki equation.
In fact, as for $v_k(\tau)$, also for this functions the Wronskian takes the form as in (2.3.13) for proper α_k and β_k coefficient, such as

$$|\alpha_k|^2 - |\beta_k|^2 = 1. \tag{2.3.23}$$

Both $u_k(\tau)$ and $v_k(\tau)$ satisfy the Mukhanov-Sasaki equation (2.3.9) and at this point nothing allows us to perform a better choice preferring one function with respect to the other, since both would be a reasonable choice. Therefore, modes can not be uniquely chosen.
The same happens in the choice of states' basis. We can expand $v_k(\tau)$ in terms of $u_k(\tau)$

$$\hat{v}(\tau, \mathbf{x}) = \int \frac{\mathrm{d}^3\mathbf{k}}{(2\pi)^{3/2}} [\hat{b}^-_{\mathbf{k}} u_k(\tau) e^{i\mathbf{k}\cdot\mathbf{x}} + \hat{b}^+_{\mathbf{k}} u^*_k(\tau) e^{-i\mathbf{k}\cdot\mathbf{x}}], \tag{2.3.24}$$

where $\hat{a}^{\pm}_{\mathbf{k}}$ and $\hat{b}^{\pm}_{\mathbf{k}}$ are both creation/annihilation operators, but form different bases in the Hilbert space:

$$\hat{a}^{-}_{\mathbf{k}} \left|0\right\rangle_a = 0, \quad \left|m_{\mathbf{k}}, n_{\mathbf{p}}, ...\right\rangle_a = \frac{1}{\sqrt{m!n!...}} \left[(\hat{a}^{+}_{\mathbf{k}})^m (\hat{a}^{+}_{\mathbf{p}})^n ...\right] \left|0\right\rangle_a \tag{2.3.25}$$

$$\hat{b}^{-}_{\mathbf{k}} \left|0\right\rangle_b = 0, \quad \left|m_{\mathbf{k}}, n_{\mathbf{p}}, ...\right\rangle_b = \frac{1}{\sqrt{m!n!...}} \left[(\hat{b}^{+}_{\mathbf{k}})^m (\hat{b}^{+}_{\mathbf{p}})^n ...\right] \left|0\right\rangle_b . \tag{2.3.26}$$

The choice we may perform on the vacuum is not unique, since we proved there exists another equivalent but different basis.

Between these two operators a Bogolyubov transformation can be performed in order to pass from one basis to the other

$$\hat{a}^{-}_{\mathbf{k}} = \alpha^{*}_{k} \hat{b}^{-}_{\mathbf{k}} + \beta_k \hat{b}^{+}_{\text{-}\mathbf{k}} \tag{2.3.27}$$

$$\hat{a}^{+}_{\mathbf{k}} = \alpha_{k} \hat{b}^{+}_{\mathbf{k}} + \beta^{*}_k \hat{b}^{-}_{\text{-}\mathbf{k}}. \tag{2.3.28}$$

Since different vacua can be chosen, let us consider two example that would be useful later.

Vacuum in Minkowski Space In the Minkowsi space the (2.3.9) becomes

$$v''_k + k^2 v_k = 0. \tag{2.3.29}$$

In a time-independent spacetime we can define a unique physical vacuum $\left|0\right\rangle_v$ requiring that in this vacuum state the expectation value of the Hamiltonian ${}_v\left\langle 0\right| \hat{H} \left|0\right\rangle_v$ is minimized.
The Hamiltonian is given by

$$\hat{H} = \frac{1}{2} \int \mathrm{d}^3\mathbf{k} \left[\hat{a}^{-}_{\mathbf{k}} \hat{a}^{-}_{\text{-}\mathbf{k}} F^{*}_k + \hat{a}^{+}_{\mathbf{k}} \hat{a}^{+}_{\text{-}\mathbf{k}} F_k + (2\hat{a}^{+}_{\mathbf{k}} \hat{a}^{-}_{\mathbf{k}} + \delta(0)) E_k\right], \tag{2.3.30}$$

where

$$E_k \equiv |v'_k|^2 + k^2 |v_k|^2 \tag{2.3.31}$$

$$F_k \equiv v'^2_k + k^2 v^2_k. \tag{2.3.32}$$

Using the first relations in (2.3.20), the only non vanishing term for ${}_v\left\langle 0\right| \hat{H} \left|0\right\rangle_v$ is given by the Hamiltonian

$$\hat{H} = \frac{1}{2} \int \mathrm{d}^3\mathbf{k}\ \delta(0) E_k \tag{2.3.33}$$

and the expectation value we get is

$${}_v\left\langle 0\right| \hat{H} \left|0\right\rangle_v = \frac{\delta(0)}{2} \int \mathrm{d}^3\mathbf{k}\ E_k. \tag{2.3.34}$$

Since $\delta(0)$ arises due to the fact that we are considering an infinite spatial volume, it is convenient to stick to the energy density

$$\varepsilon = \frac{1}{2}\int \mathrm{d}^3\mathbf{k}\ E_k \tag{2.3.35}$$

and it is clearly minimized when E_k is minimized.
Writing the modes and their first time-derivatives as $v_k = r_k e^{i\alpha_k}$ and $v_k' = r_k e^{i\alpha_k}(i\alpha_k) + r_k' e^{i\alpha_k}$, from (2.3.31) we have

$$\begin{aligned} E_k &= r_k'^2\left|e^{i\alpha_k}\right|^2 + r_k^2\left|(i\alpha_k')e^{i\alpha_k}\right|^2 + k^2 r_k^2\left|e^{i\alpha_k}\right|^2 \\ &= r_k'^2 + r_k^2\alpha_k'^2 + k^2 r_k^2 \\ &= r_k'^2 + \frac{1}{4r_k^2} + k^2 r_k^2, \end{aligned} \tag{2.3.36}$$

which reaches its minimum value for $r_k' = 0$ and $r_k = 1/\sqrt{2k}$.
From (2.3.13) we know $v_k' v_k^* - v_k v_k'^* = -i$, which gives

$$r_k^2\alpha_k' = -\frac{1}{2}, \tag{2.3.37}$$

that, once integrated, yields $\alpha_k = -k\tau$ and permit us to write the modes as

$$v_k(\tau) = \frac{1}{\sqrt{2k}}e^{-ik\tau}. \tag{2.3.38}$$

Bunch-Davies Vacuum In a quasi-de Sitter space all the modes have time-independent frequencies in remote past, therefore they behave just like in Minkowski space not being affected by gravity. This happens because, if a curved space interval small enough is considered, it can be analysed as it was flat, and hence it can be treated as Minkowski space. For this case the solution has already been calculated in the paragraph above.
The Minkowski initial condition for the mode functions is enough to avoid the non-uniqueness of vacuum and permit us to solve the Mukhanov-Sasaki equation with the initial condition

$$\lim_{\tau\to-\infty} v_k(\tau) = \frac{1}{\sqrt{2k}}e^{-ik\tau}. \tag{2.3.39}$$

2.3.3 The Power spectrum

In a perfect de Sitter space $a = -(H\tau)^{-1}$, hence the effective frequency reduces to $\omega_k^2(\tau) = k^2 - 2/\tau^2$. Therefore in this space the Mukhanov-Sasaki equation takes the form

$$v_k'' + \left(k^2 - \frac{2}{\tau^2}\right)v_k = 0. \tag{2.3.40}$$

The exact solution is given by

$$v_k(\tau) = \alpha \frac{e^{-ik\tau}}{\sqrt{2k}} \left(1 - \frac{i}{k\tau}\right) + \beta \frac{e^{ik\tau}}{\sqrt{2k}} \left(1 + \frac{i}{k\tau}\right). \tag{2.3.41}$$

The initial condition (2.3.39) set $\beta = 0$ and $\alpha = 1$, therefore the (2.3.41) becomes

$$v_k = \frac{e^{-ik\tau}}{\sqrt{2k}} \left(1 - \frac{i}{k\tau}\right). \tag{2.3.42}$$

It is possible to evaluate the effect of quantum zero-point fluctuations:

$$\begin{aligned}
\langle 0| \hat{v}_k \hat{v}_{k'} |0\rangle &= \langle 0| (a^-_{\mathbf{k}} v_k + a^+_{\text{-}\mathbf{k}} v^*_k)(a^-_{\mathbf{k}}, v_{k'} + a^+_{\text{-}\mathbf{k}}, v^*_{k'}) |0\rangle \\
&= v_k v^*_{k'} \langle 0| a^-_{\mathbf{k}} a^+_{\text{-}\mathbf{k}} |0\rangle \\
&= v_k v^*_{k'} \langle 0| \left([a^-_{\mathbf{k}}, a^+_{\text{-}\mathbf{k}}] - a^+_{\text{-}\mathbf{k}} a^-_{\mathbf{k}}\right) |0\rangle \\
&= |v_k|^2 \delta(\mathbf{k} + \mathbf{k'}) \qquad (2.3.43) \\
&= P_v(k) \delta(\mathbf{k} + \mathbf{k'}) \qquad (2.3.44)
\end{aligned}$$

where $P_v(k)$ is the power spectrum for field in de Sitter space. It is important to state that this type of power spectrum is not physical, since it describes a never ending inflation. For this reason, we have to consider curvature perturbations ζ, in order to deviate from the de Sitter space during inflation and therefore let it end. Curvature perturbations are meaningless in perfect de Sitter space, because in this space $\zeta = z^{-1}v$ can not be properly defined since z vanishes. In quasi-de Sitter space the power spectrum of the curvature perturbations, from equation (2.3.43), is

$$P_\zeta = \frac{1}{z^2} P_v = \left|\frac{v_k}{z}\right|^2 \tag{2.3.45}$$

and in its dimensionless form it becomes

$$P_k = \frac{k^3}{2\pi^2} \left|\frac{v_k}{z}\right|^2, \tag{2.3.46}$$

which gives us the amplitude of the power spectrum.

On super-horizon scales the curvature perturbations remain constant and the two-point function can therefore be evaluated at horizon crossing $k = aH$. On super-horizon $P_v = (aH)^2/(2k^3)$, hence

$$P_k = \frac{1}{8\pi^2} \frac{H}{\varepsilon}\Big|_{k=aH}. \tag{2.3.47}$$

Besides the amplitude, another crucial parameter to be considered is the spectral index, which quantifies how much the power spectrum P_ζ deviates from its scale invariant form

P_k, and it is defined as

$$\begin{aligned} n_s - 1 &\equiv \frac{d\ln P_k}{d\ln k} \\ &= \frac{d\ln P_k}{d\ln N}\frac{d\ln N}{d\ln k} \\ &= \left(2\frac{d\ln H}{dN} - \frac{d\ln \varepsilon}{dN}\right)\frac{d\ln N}{d\ln k} \\ &= (-2\varepsilon - \eta)\frac{d\ln N}{d\ln k}. \end{aligned} \tag{2.3.48}$$

The last term can be evaluated using the horizon crossing condition $k = aH$ and the definition of $N = \ln a$:

$$\ln k = N + \ln H \tag{2.3.49}$$

$$\frac{d\ln N}{d\ln k} = \left[\frac{d\ln k}{d\ln N}\right]^{-1} = \tag{2.3.50}$$

$$= \left[1 + \frac{d\ln H}{d\ln N}\right]^{-1} \tag{2.3.51}$$

$$= [1-\varepsilon]^{-1} \approx 1 + \varepsilon \tag{2.3.52}$$

therefore n_s can be written as

$$n_s - 1 = (-2\varepsilon - \eta)(1 + \varepsilon), \tag{2.3.53}$$

that reduces to

$$n_s - 1 = -2\varepsilon - \eta \tag{2.3.54}$$

at its first order.

Experimental constraints are set on P_k and n_s:

$$P_k^{CMB} = 2 \cdot 10^{-9} \tag{2.3.55}$$

$$n_s = 0.9650 \pm 0.0050 \tag{2.3.56}$$

$$\frac{\mathrm{d}n_s}{\mathrm{d}\ln k} = -0.009 \pm 0.008, \tag{2.3.57}$$

where P_k^{CMB} is P_k evaluated at the CMB scale, while n_s and the running $\frac{\mathrm{d}n_s}{\mathrm{d}\ln k}$ are evaluated at pivot scale $k_* = 0.05$ Mpc^{-1} at 68%CL [11].

Chapter 3

Primordial Power Spectrum and PBH Dark Matter

In the early 1970s S. Hawking and Y. B. Zeldovich independently proposed that overdense inhomogeneities in the early universe could lead to gravitational collapse and the formation of Primordial Black Holes (PBHs). Forming during radiation-dominated era when fluctuations with sufficiently large amplitude re-enter the horizon and undergo gravitational collapse, PBHs could contribute to the present dark matter abundance. For PBHs to be a significant contribution to the dark matter fraction the power spectrum at small scales needs to be enhanced by several orders of magnitude with respect to its value on CMB scales.
Today the idea of PBHs constituting a significant fraction of dark matter has become more and more present, because this sort of mechanism for dark matter production does not require any beyond the Standard Model physics or particle.
Constraints are set on the masses range that PBHs can have, in order for them to describe a total or partial fraction of dark matter. This vast range is limited from below by Hawking radiation, since very light PBHs ($M \lesssim 10^{-17} M_\odot$) would have entirely evaporated by now. As upper bounds several experimental measurements have excluded some values from the masses range, see Figure 3.1.

In this dissertation we will focus on PBHs with masses in the range $10^{-17} M_\odot \lesssim M \lesssim 10^{-14} M_\odot$. In this range PBHs can make up between 10% and 100% of dark matter.

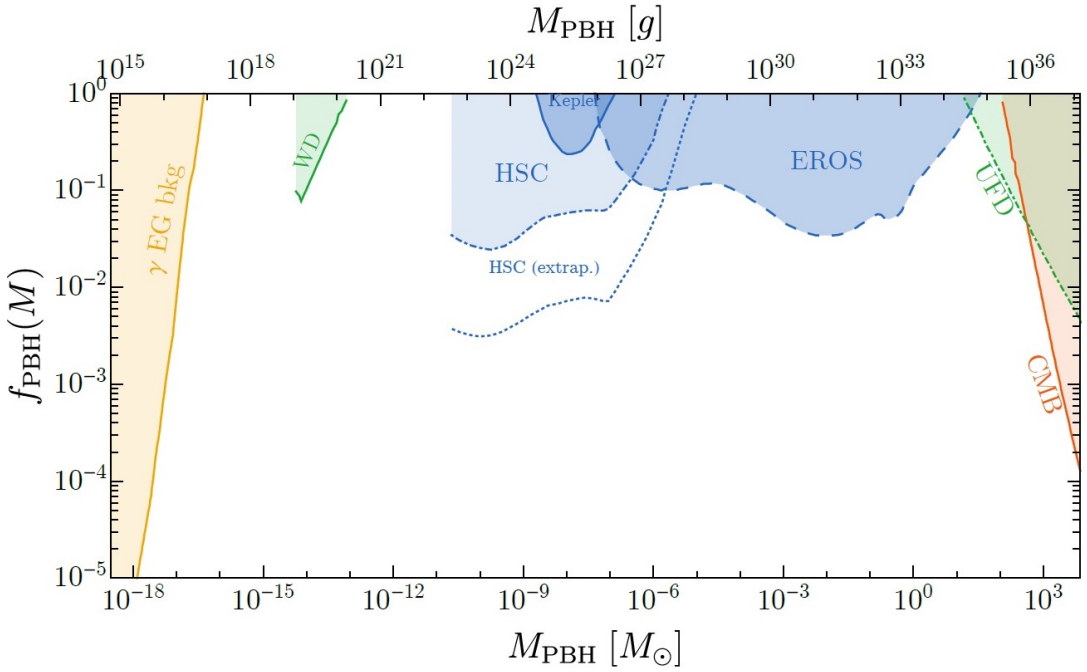

Figure 3.1: The diagram shows the current experimental constraints on PBHs mass. Different bounds are shown: the extra-galactic γ-ray background (yellow); the micro- and milli- lensing observations from Fermi, Eros, Kepler, Subaru HSC (blue); the dynamical constraints from White Dwarves and Ultra-Faint Dwarf galaxies (green); the constraints from the CMB (orange). The LISA observatory is now investigating PBHs around $M \sim 10^{-12} M_\odot$. Source [12].

3.1 PBH Formation

The total energy density of PBHs with mass M at their formation[13][14][15] is given by

$$\beta_f(M) \equiv \left. \frac{\rho_{PBH}}{\rho_{tot}} \right|_f . \tag{3.1.1}$$

The probability for curvature perturbations to form PBHs with mass M is assumed to follow a Gaussian distribution with standard deviation $\sigma_M \equiv \sigma(M)$, hence

$$\beta_f(M) = \int_{\zeta_c}^{\infty} \frac{1}{\sqrt{2\pi}\sigma_M} e^{-\frac{\zeta^2}{2\sigma_M^2}} \mathrm{d}\zeta, \tag{3.1.2}$$

where ζ_c is the critical value for mass to collapse into PBH.
A typical value for ζ in the Gaussian approximation is $\zeta_c = 1$, therefore we can approxi-

mate the equation (3.1.2) as

$$\beta_f(M) \approx \frac{\sigma_M}{\sqrt{2\pi}\zeta_c} e^{-\frac{\zeta_c^2}{2\sigma_M^2}}. \tag{3.1.3}$$

For non-Gaussian case, see [16].
A constraint must be set on the smallness of σ_M, since PBHs are created to be a significant fraction of dark matter, hence the fluctuations that collapse to from them can not be too rare.

Since PBHs behave as matter, we can study the fraction of their total energy density at their formation

$$\beta_f(M) = \left(\frac{H_0}{H_f}\right)^2 \frac{\Omega_{DM0}}{a_f^3} f_{PBH}(M), \tag{3.1.4}$$

where a_f is the scale factor at formation time, $f_{PBH}(M)$ is the fraction of PBHs against the total dark matter and Ω_{DM} is the density parameter for dark matter, which today is $\Omega_{DM0} \approx 0.26$.

The mass of a PBH is assumed to be proportional to the horizon mass M_H

$$M = \gamma M_H = \gamma \frac{4\pi}{3} \frac{\rho_{tot}}{H^3}\Big|_f, \tag{3.1.5}$$

where γ is a correction factor associated with the gravitational collapse rate.
Using $H^2 = \rho_{tot}/(3M_p^2)$, we can write (3.1.5) as

$$M = 4\pi\gamma \frac{M_p^2}{H_f}, \tag{3.1.6}$$

where H_f the Hubble parameter evaluated at formation time, i.e. when perturbations re-enter the horizon.
Let us see how we can write H_f, taking into account that the formation of PBHs occurs in a radiation-dominated universe. Using the conservation of entropy $S = a^3 s \approx a^3 g_* T^3$, we can find the radiation density

$$\rho_{rad} \approx g_* T^4 \approx g_* a_f^{-4} \left(\frac{g_{*0}}{g_*}\right)^{1/3} T_0^4 \tag{3.1.7}$$

and therefore the radiation density parameter today

$$\Omega_{rad0} = \frac{\rho_{rad0}}{\rho_{crit0}} \approx \frac{g_{*0} T_0^4}{3M_p^2 H_0^2} \tag{3.1.8}$$

from which we can obtain a relation for T_0 and therefore write the Hubble parameter at formation as

$$H_f^2 = \frac{\rho_{rad}}{3M_p^2} \approx \left(\frac{g_*}{g_{*0}}\right)^{-1/3} a_f^{-4} \Omega_{rad0} H_0^2. \tag{3.1.9}$$

where $\Omega_{rad0} = 8 \cdot 10^{-5}$, while g_{*f} and g_{*0} are the number of degrees of freedom at formation time and today respectively.

Using the equation (3.1.6) together with 3.1.9, $\beta_f(M)$ in (3.1.4) takes the form

$$\beta_f(M) \sim \frac{4}{\sqrt{\gamma}} \cdot 10^{-9} \left(\frac{g_{*f}}{g_{*0}}\right)^{1/4} \sqrt{\frac{M}{M_\odot}} f_{PBH}(M). \tag{3.1.10}$$

We can now evaluate it setting $\gamma = 1$ ($M = M_H$) and $f_{PBH}(M) = 1$, for PBHs constituting the totality of dark matter, and assuming only SM degrees of freedom are present, namely $g_{*f} = 106.75$ and $g_{*0} = 3.36$:

$$\beta_f(M) \approx 10^{-8} \sqrt{\frac{M}{M_\odot}}, \tag{3.1.11}$$

that in the case of $M = 10^{-15} M_\odot$ gives $\beta_f(M) \approx 3 \cdot 10^{-16}$.

From the equations (3.1.3) and (3.1.11), we can find $\sigma_M = 0.12$ for $\zeta_c = 1$, implying that the amplitude of the power spectrum must reach $\mathcal{O}(10^{-2})$, which is 7 order of magnitude greater than the amplitude on the CMB scale (2.3.55).
This enhancement can be obtained in single field inflation framework by considering a model based on a potential with an extremely flat and sufficiently long region.

3.2 Fibre Inflation Potential

Fibre inflation [17][14] is a class of string inflationary models built within the framework of type IIB flux compactifications [10][18]. The simplest model of fibre inflation is obtained considering a Calabi-Yau volume

$$\mathcal{V} = t_{\mathbb{P}^1} \tau_{K3} - \tau_{\mathrm{d}P}^{3/2}, \tag{3.2.1}$$

where $\tau_{\mathrm{d}P}$ is the volume of diagonal del Pezzo divisor and τ_{K3} is the Kähler modulus over the base $\mathbb{P}^1$ with volume $t_{\mathbb{P}^1}$.
The flat direction τ_{K3} is a valid candidate to represent the inflaton.
$\mathcal{V}$ and $\tau_{\mathrm{d}P}$ do not play a significant role during inflation, which is mainly driven by the

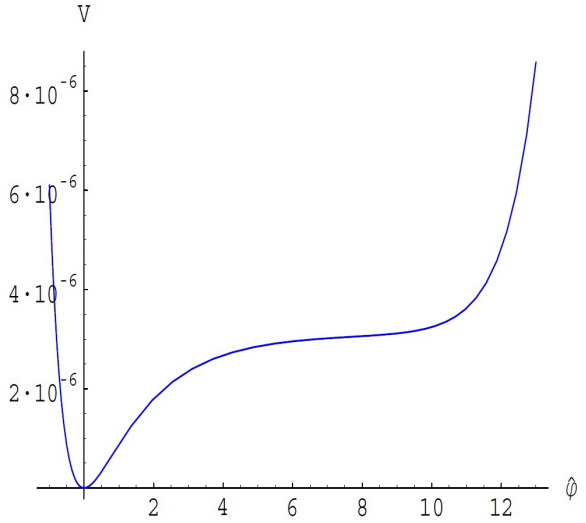

Figure 3.2: Fibre inflationary potential. It can be noticed a minimum at small scale, a plateau-like behaviour at large scale and the fast-roll phase at larger scales. The graph is evaluated for the set of value found in [17].

field τ_{K3}, hence fibre inflation models can be well approximated to a single-field inflation model, whose potential takes the form

$$V_{inf} = \frac{W_0^2}{\mathcal{V}^2}\left(\frac{C_{up}}{\mathcal{V}^{4/3}} + g_s^2\frac{C_{KK}}{\tau_{K3}^2} + \frac{W_0^2}{\sqrt{g_s}}\frac{\epsilon_{F^4}}{\mathcal{V}\tau_{K3}} - \frac{C_W}{\mathcal{V}\sqrt{\tau_{K3}}} + g_s^2 D_{KK}\frac{\tau_{K3}}{\mathcal{V}^2} + \delta_{F^4}\frac{W_0^2}{\sqrt{g_s}}\frac{\sqrt{\tau_{K3}}}{\mathcal{V}^2}\right), \tag{3.2.2}$$

where $g_s \ll 1$ is the string coupling constant; W_0 is the superpotential generated by background fluxes; C_{up} is a constant controlling the uplifting contribution; $C_{KK} > 0$, $D_{KK} > 0$ and C_W are coefficients of 1-loop opens string correction, are functions of the vacuum expectation values of the complex structure moduli and are expected to be $C_{KK} \sim D_{KK} \sim C_W \sim \mathcal{O}(1)$; $\epsilon_{F^4} \sim \delta_{F^4} \sim \mathcal{O}(10^{-3})$ are positive but small coefficient depending only on the topology of the considered space geometry.

A potential of this form presents three distinct behaviours: for small τ_{K3} it features a minimum, for large τ_{K3} an inflationary plateau and for very large τ_{K3} a fast-roll regime region, see Figure 3.2.

By writing τ_{K3} using the canonically normalized inflaton with ϕ, we obtain

$$\tau_{K3} = e^{\frac{2}{\sqrt{3}}\phi} = \langle\tau_{K3}\rangle e^{\frac{2}{\sqrt{3}}\hat{\phi}}, \tag{3.2.3}$$

where ϕ has been expanded around its minimum $\phi = \frac{2}{\sqrt{3}} \ln\langle\tau_{K3}\rangle + \hat{\phi}$.
Substituting (3.2.3) in (3.2.2), we have

$$V_{inf} = V_0 \left(C_1 + C_2 e^{-\frac{4}{\sqrt{3}}\hat{\phi}} + C_3 e^{-\frac{2}{\sqrt{3}}\hat{\phi}} - e^{-\frac{1}{\sqrt{3}}\hat{\phi}} + C_4 e^{\frac{2}{\sqrt{3}}\hat{\phi}} + C_5 e^{\frac{1}{\sqrt{3}}\hat{\phi}} \right), \tag{3.2.4}$$

where all the numerical constant can be wittren by parameterising the inflaton minimum $\langle\tau_{K3}\rangle^{3/2} \equiv \gamma\mathcal{V}$:

$$V_0 = \frac{C_W W_0^2}{\gamma^{1/3}\mathcal{V}^{10/3}} \tag{3.2.5}$$

$$C_1 = \gamma^{1/3}\frac{C_{up}}{C_W} \tag{3.2.6}$$

$$C_2 = g_S^2 \frac{C_{KK}}{\gamma C_W} \tag{3.2.7}$$

$$C_3 = \frac{W_0^2}{\gamma^{1/3} C_W \sqrt{g_s}} \frac{\epsilon_{F^4}}{\mathcal{V}^{1/3}} \tag{3.2.8}$$

$$C_4 = \gamma g_s^2 \frac{D_{KK}}{C_W} \tag{3.2.9}$$

$$C_5 = \gamma C_3 \frac{\delta_{F^4}}{\epsilon_{F^4}}. \tag{3.2.10}$$

In order for the potential to have a plateau region which can support enough e-folds of inflation, we must have $C_4 \ll 1$ and $C_5 \ll 1$, hence $\gamma \ll 1$. This is naturally achieved when $\gamma \sim g_s^2$, i.e. when the three negative exponential terms compete to give a minimum. On the other hand, the inflationary plateau is mainly generated by the fourth term.

3.2.1 Ultra Slow-Roll Background for PBH

This type of potential is valid to describe inflation, but not to form PBHs because it does not have enough structure to induce the enhancement on small scales required in the power spectrum amplitude. We will use a generalization [14] of it: C_W will be promoted from a constant to a function of τ_{K3}

$$C_W(\tau_{K3}) = C_W - \frac{A_W\sqrt{\tau_{K3}}}{\sqrt{\tau_{K3}} - B_W}, \tag{3.2.11}$$

where $C_W \sim A_W \sim B_W \sim \mathcal{O}(1)$. A_W depends on the vacuum expectation values of the complex structure and B_W on the topology of the Calabi-Yau manifold. Moreover, a further generalization is yielded by an additional winding 1-loop correction to the potential

$$\delta V_W = W_0^2 \frac{\tau_{K3}}{\mathcal{V}^4} \left(D_W - \frac{G_W}{1 + R_W \frac{\tau_{K3}^{3/2}}{\mathcal{V}}} \right), \tag{3.2.12}$$

where $D_W \sim G_W \sim R_W \sim \mathcal{O}(1)$. G_W becomes constant only after complex structure of moduli stabilisation and R_W depends on the topology of extra dimensions. This term will be crucial for PBHs formation.

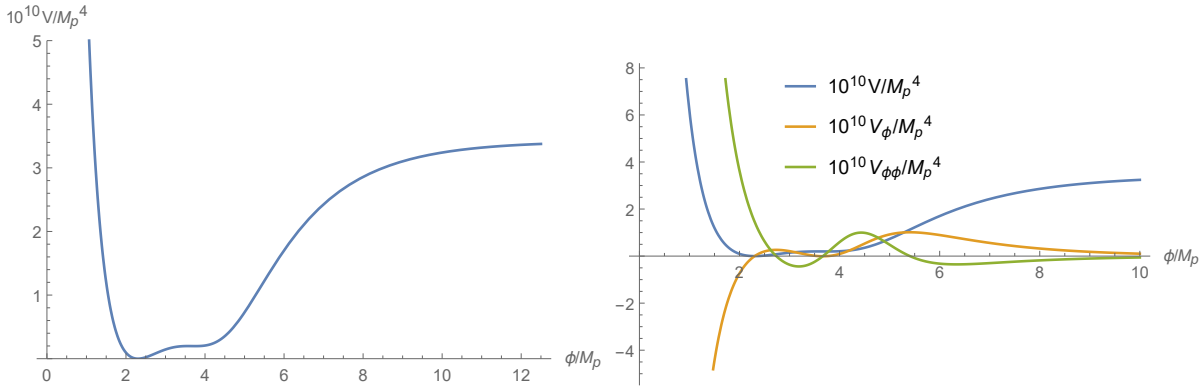

Figure 3.3: Left: The image shows the scalar potential for set $\mathcal{P}_2$. Right: The image shows the potential (blue line) and its first (green line) and second (orange line) derivatives near the minimum and the plateau, both as function of the canonically normalized field and obtained through the set $\mathcal{P}_2$ in Table 3.1. The PBH plateau region can be seen in $2.7 < \phi/M_p < 4$, while the post-inflationary minimum lies around $\phi = 2.3$

Sticking to a simple situation where just the winding 1-loop correction is considered, i.e. $C_{KK} = D_{KK} = 0$, and where higher derivative F^4 are negligible, the potential that leads to PBHs formation simplifies to

$$V_{inf} = \frac{W_0^2}{\mathcal{V}^3}\left[\frac{C_{up}}{\mathcal{V}^{1/3}} - \frac{C_W}{\sqrt{\tau_{K3}}} + \frac{A_W}{\sqrt{\tau_{K3}} - B_W} + \frac{\tau_{K3}}{\mathcal{V}}\left(D_W - \frac{G_W}{1 + R_W \frac{\tau_{K3}^{3/2}}{\mathcal{V}}}\right)\right]. \tag{3.2.13}$$

Now, in order to create a significant abundance of PBHs during the inflationary period, the potential must present an inflection point close to the minimum. From (3.2.13) we can see that at small τ_{K3} the second and third terms dominate and induce a minimum for the modulus

$$\langle \tau_{K3} \rangle \sim \frac{C_W B_W^2}{(\sqrt{C_W} - \sqrt{A_W})^2}, \tag{3.2.14}$$

while for large τ_{K3} the fourth dominates V. The fifth term behaves as $-\tau_{K3}$ at small field and as $-\tau_{K3}^{-1/2}$ at large field, and it has a maximum for at $\frac{2^{2/3}}{(R_W/\mathcal{V})^{2/3}}$.
As already said in the present section, the term that turns out to be crucial is the fifth: in fact, in order to obtain the enhancement needed in the power spectrum for PBHs production, this term will be tuned such that the potential presents a plateau region close to the post-inflationary minimum, see Figure 3.3.

Fibre inflation models require a trans-Planckian field range to obtain enough e-foldings of inflationary expansion, for this reason they predict a tensor-to-scalar ratio

$$r = \frac{A_\Gamma(k_*)}{A_s(k_*)}\Big|_{N_{CMB}} = 16\varepsilon \sim 0.005 - 0.01, \tag{3.2.15}$$

where r is the ratio between the tensor and the scalar power spectrum amplitude calculated at the CMB scale.

Ultra slow-Roll dynamics

The ultra slow-roll period [19] is described by an extremely flat potential, as can be seen in Figure 3.3 for $2.7 < \phi/M_p < 4$. The flatness of the potential causes a drastic reduction in its slope value, giving $V \sim const$ and hence $V_\phi \approx 0$. Thus, the equation of motion for the field ϕ described by the Lagrangian (2.2.1) simplifies to

$$\ddot{\phi} + 3H\dot{\phi} \approx 0. \tag{3.2.16}$$

The inflationary parameter η, using its own definition and the equation (2.2.10), can be written as

$$\eta = \frac{\dot{\varepsilon}}{H\varepsilon} = -6 - \frac{2V_\phi H}{\dot{\phi}} + 2\varepsilon, \tag{3.2.17}$$

that for the ultra slow-roll phase becomes

$$\eta \approx -6 + 2\varepsilon. \tag{3.2.18}$$

Since $\varepsilon < 1$ during the entire inflationary period, $\eta \sim -6$.

To summarise, the parameter $|\eta|$ is initially small but when the potential becomes very flat it tends to grow reaching values that are larger than unity ($|\eta| \sim 6$). For this reason the slow-roll approximation is no longer valid for a period of ultra slow-roll inflation.

3.2.2 Numerical results

First, we set $C_{up} = D_W = 0$, hence the potential becomes

$$V_{inf} = \frac{W_0^2}{\mathcal{V}^3}\left[\frac{-C_W}{\sqrt{\tau_{K3}}} + \frac{A_W\sqrt{\tau_{K3}}}{\sqrt{\tau_{K3}} - B_W} + \frac{\tau_{K3}}{\mathcal{V}}\left(\frac{G_W}{1 + R_W\frac{\tau_{K3}^{3/2}}{\mathcal{V}}}\right)\right]. \tag{3.2.19}$$

The background is analysed as in section 2.2 solving both the Friedmann (2.2.8) and

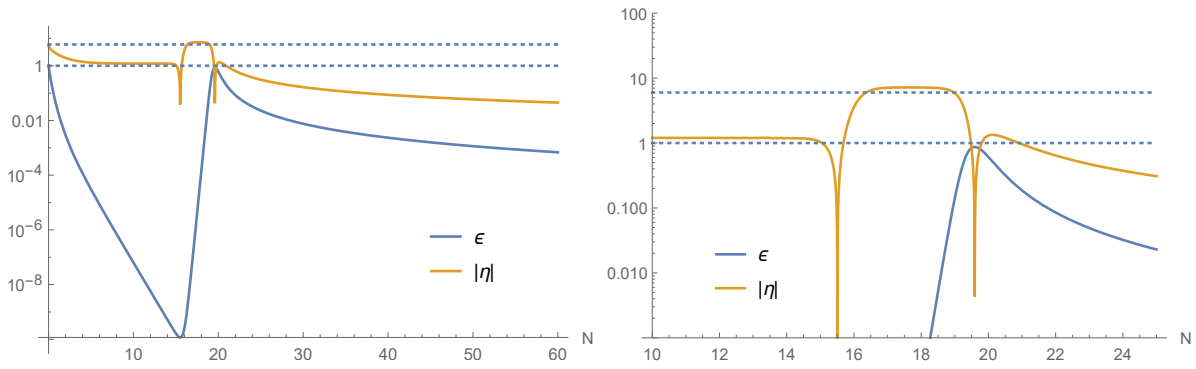

Figure 3.4: Left: The image shows the behaviour of the slow-roll parameters ε (blue line) and η (orange line) for $\mathcal{P}_2$ as functions of the e-folds number N in the complete domain of inflation. Right: from 10 to 25 e-folds. For $N > 19$ the system undergoes a slow-roll phase, for $15 < N < 19$ it enters the ultra slow-roll phase with η reaching 6, and finally for $N < 15$ the system faces a second slow-roll phase with $\eta = \mathcal{O}(1)$. At $N = 0$ inflation ends.

the Klein-Gordon equations (2.2.5).
On the other hand, in the plateau the physics deviates significantly from slow-roll inflation, entering a region with ultra slow-roll dynamics. For this reason, the power spectrum amplitude and the spectral index must be calculated through the Mukhanov-Sasaki equation (2.3.9), because in the slow-roll approximation these values would be drastically underestimated. The effective mass of curvature perturbations can be expanded as

$$\frac{z''}{z} = (aH)^2 \left[2 - \varepsilon + \frac{3}{2}\eta - \frac{1}{2}\varepsilon\eta + \frac{1}{4}\eta^2 + \frac{1}{2}\eta\kappa\right], \tag{3.2.20}$$

where $\kappa = \dot{\eta}/(\eta H)$. Therefore the (2.3.9) is computed and as initial conditions the Bunch-Davies limit (2.3.39) is taken.

From Figure 3.4 it is clear that the inflationary period can be divided in three different phases: for $N > 19$ the system undergoes a slow-roll period, transitioning then for $15 < N < 19$ to an ultra slow-roll phase and lastly for $N < 15$ to a second slow-roll period, which this time is characterized by a large value of η.
It is useful to evaluate the difference between the e-folds number corresponding to the PBH and the CMB scales leaving the horizon [20]:

$$\Delta N_{CMB}^{PBH} = \ln\left(\frac{a_f}{a_{CMB}}\right) = \ln\left(\frac{a_f H_f}{a_{CMB} H_f}\right) = \ln\left(\frac{a_f H_f}{k_*}\right). \tag{3.2.21}$$

Using the equations (3.1.9) for the Hubble parameter and (3.1.6) for the PBHs mass, which can be written as a function of the gravitational constant $M = \gamma \frac{1}{2GH_f}$, the equation

(3.2.21) becomes

$$\Delta N_{CMB}^{PBH} \approx \ln\left[\left(\frac{M}{M_\odot}\right)^{-1/2}\left(\frac{g_*}{g_{*0}}\right)^{-1/12}\Omega_{rad0}^{1/4}\left(\frac{2G}{\gamma}M_\odot\right)^{-1/2}H_0^{1/2}\frac{1}{k_*}\right] \tag{3.2.22}$$

$$= 18.4 - \frac{1}{12}\ln\frac{g_*}{g_{*0}} + \frac{1}{2}\ln\gamma - \frac{1}{2}\ln\frac{M}{M_\odot}. \tag{3.2.23}$$

Evaluating it in $\Omega_{rad0} = 8\cdot 10^{-5}$, $\gamma = 1$ and assuming only SM degrees of freedom are present $g_{*f} = 106.75$ and $g_{*0} = 3.36$, for PBHs with masses around $10^{-16}M_\odot - 10^{-14}M_\odot$ the PBH scales leave the horizon approximately after 34.2-36.5 e-folds the CMB scales.

We find now the scalar power spectrum as in (2.3.46), evaluated at the end of inflation, and the spectral index as defined in (2.3.48).
Numerical results can be found in Table 3.2. These numerical examples are calculated assuming $\zeta_c = 1$ for PBHs with masses a few times $10^{-15}M_\odot$, which leads to $\Delta N_{CMB}^{PBH} = 35$.

	$\mathcal{P}_1$	$\mathcal{P}_2$	$\mathcal{P}_3$	$\mathcal{P}_4$
W_0	$1.04\cdot 10^{-1}$	9.47	$1.85\cdot 10^{4}$	1.60
C_W	1/10	4/100	1.978/100	17/100
A_W	2/100	2/100	1.65/100	8/100
B_W	1	1	1.01	1
$G_W/\mathcal{V}$	$1.303386\cdot 10^{-3}$	$3.080548\cdot 10^{-5}$	$9.257715\cdot 10^{-8}$	$1.8001844\cdot 10^{-4}$
$R_W\mathcal{V}$	$6.58724\cdot 10^{-3}$	$7.071067\cdot 10^{-4}$	$1.414\cdot 10^{-5}$	$9.1079272\cdot 10^{-4}$
$\mathcal{V}$	107.3	1000	$5\cdot 10^{4}$	550
$\langle\tau_{K3}\rangle$	3.88738	14.2957	168.033	12.4865

Table 3.1: Numerical values for parameters in the potential (3.2.19).

	$\mathcal{P}_1$	$\mathcal{P}_2$	$\mathcal{P}_3$	$\mathcal{P}_4$
n_s	0.9473	0.9447	0.9460	0.9467
$P_k\vert_{peak}$	0.01985	0.0609513	0.0223268	0.0386759
Δ_{CMB}^{PBH}	35	35	35	35
r	0.00904034	0.0109949	0.0143309	0.0098281

Table 3.2: Observables n_s and P_k evaluated in the peak at PBH scales for the scalar power spectrum obtained through the sets presented in Table 3.1.

As expected, the slow-roll approximation is no longer valid for modes that cross the horizon near the ultra slow-roll region. The power spectrum for modes leaving the horizon

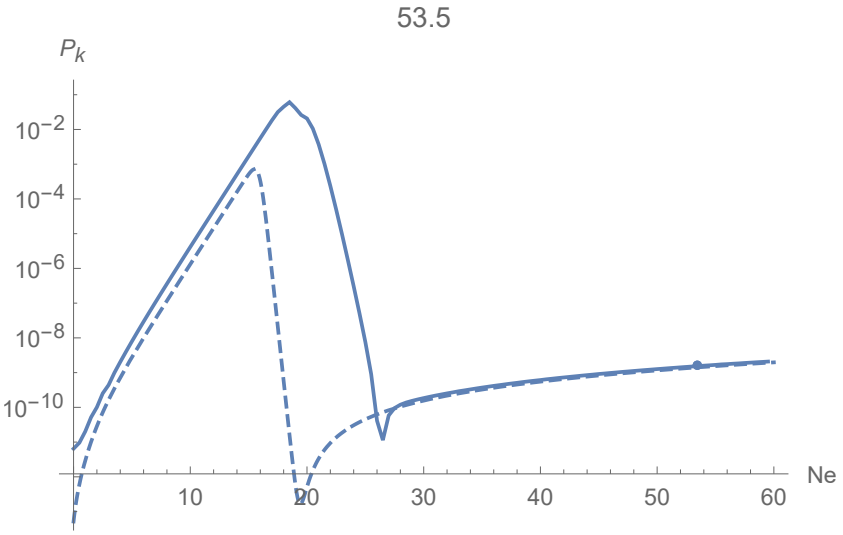

Figure 3.5: Scalar power spectrum evaluated at the end of inflation for the set $\mathcal{P}_2$. The continuous line has been obtained through the solution of Mukhanov-Sasaki equation, while the dotted line represents the slow-roll approximation. The e-folds number at which n_s is calculated is written in the upper part of the graph and it is represented in the graph by the dot.

before and after the ultra slow-roll transition are shown in Figure 3.6.
In the first case, the CMB scale modes case, the evolution of the power spectrum follows the slow-roll estimate of (2.3.47), remaining constant after crossing the horizon, while in the second, the PBH scale case, the modes leaving the horizon during the ultra slow-roll phase undergo super-horizon growth and therefore these modes cannot be described by the background physics. This behaviour for small scales can be attributed to the fact that $\eta \sim -6$ in the ultra slow-roll phase, see Figure 3.4.

We stress that the choices of the microphysical parameters are in line with expectations and that the values of the compactification volume $\mathcal{V}$ has no constraints from the request that PBHs form the total present dark matter. For different sets it can in fact take values that differ for many orders of magnitude, as it can be seen from Table 3.3. All examples lead to a spectral index that lies outside the observational range by about 2 to 3 sigma with respect to the current best fit (2.3.56), while giving rise to a spectral running and a tensor fraction that are in line with current bounds.

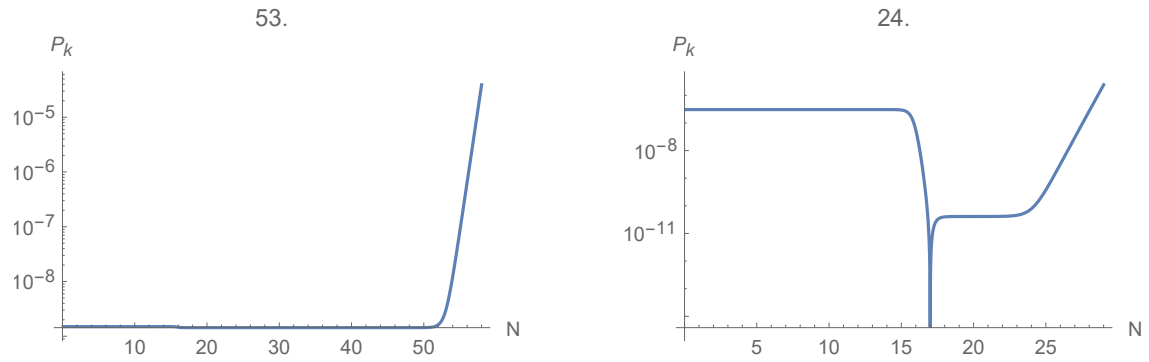

Figure 3.6: Left: The power spectrum for modes scales that leave the horizon 53 e-fold before the end of inflation, i.e. at CMB scales. Right: The power spectrum for modes scales that leave the horizon 24 e-fold before the end of inflation, i.e. at PBH scales. On the upper part of both graphs the number of e-folds at which they exit the horizon is showed. Both figures are obtained using the parameters in set $\mathcal{P}_2$.

Results for alternative models

Other models for PBHs formation have been proposed over the past year. The specific cases are reported and analysed below. In order to obtain the power spectrum and its observables, for the following models the same analysis' approach for the fibre inflation model is used.

- The first model we consider is the one proposed in [21]. This model is based on a single-field model constructed as a ratio of polynomials

$$V(\phi) = \left(\frac{1}{2}m^2\phi^2 - \frac{1}{3}\alpha v\phi^3 + \frac{1}{4}\lambda\phi^4\right)(1+\xi\phi^2)^{-2}, \tag{3.2.24}$$

  where m, α, v, λ, ξ are assumed to be constants.

  As in the string case, this potential presents a plateau-like region associated with the ultra-slow roll inflation.

  The results obtained in [21] are the following

$$n_s = 0.951 \tag{3.2.25}$$

$$\frac{\mathrm{d}n_s}{\mathrm{d}\ln k} = -0.0018 \tag{3.2.26}$$

$$r = 0.013, \tag{3.2.27}$$

where $\Delta N_{CMB}^{PBH} = 35$ is used.

These results are qualitatively similar to the ones of section 3.2.2: there is a tension in the spectral index n_s values, while the spectral running $\frac{\mathrm{d}n_s}{\mathrm{d}\ln k}$ and the tensor to scalar ratio r are in line with the observational constraints.

- The second model we are going to consider is the one in [22]. It is based on potentials that are polynomial combinations of the field ϕ. Two examples of this sort of potential are

$$V(\phi) = a_2\phi^2 - a_3\phi^3 + a_4\phi^4 \tag{3.2.28}$$

$$V(\phi) = \frac{\lambda_0}{4!}\left[1 + q_1 \ln\frac{\phi^2}{\phi_0^2} + q_2\left(\ln\frac{\phi^2}{\phi_0^2}\right)^2 + ...\right]\phi^4, \tag{3.2.29}$$

where $a_2, a_3, a_4, \lambda_0, \phi_0$ are assumed to be constants.

The results obtained for the two sets in [22] are the following

$$\begin{array}{c|c} n_s = 0.9531 \\ \frac{\mathrm{d}n_s}{\mathrm{d}\ln k} = -0.0016 \\ r = 0.036 \end{array} \quad \begin{array}{c} n_s = 0.9503 \\ \frac{\mathrm{d}n_s}{\mathrm{d}\ln k} = -0.0018 \\ r = 0.027 \end{array}$$

where $\Delta N_{CMB}^{PBH} \simeq 33$.

Also for this case, results are likely to the ones obtained for the fibre inflation model. A tension in the spectral index n_s values is still present, while the spectral running $\frac{\mathrm{d}n_s}{\mathrm{d}\ln k}$ and the tensor to scalar ratio r are in line with the observational constraints.

- The third and last model we are reviewing is the [23].
This model is described by the axion potential originated from string theory

$$V(\phi) = V_0 + \frac{1}{2}m^2\phi^2 + \Lambda_1^4\frac{\phi}{f}\cos\left(\frac{\phi}{f}\right) + \Lambda_2^4\sin\left(\frac{\phi}{f}\right). \tag{3.2.30}$$

The following parameters $\beta_i \equiv \Lambda_i^4/m^2f^2$ and f are used to evaluate the first set of values for n_s, $\frac{\mathrm{d}n_s}{\mathrm{d}\ln k}$ and r in the power spectrum

$$\beta_1 \simeq 0.86,\ \beta_2 \simeq 0.25,\ M_p/f \simeq= 1.6,\ \phi_0 = 11.55\ M_p, \tag{3.2.31}$$

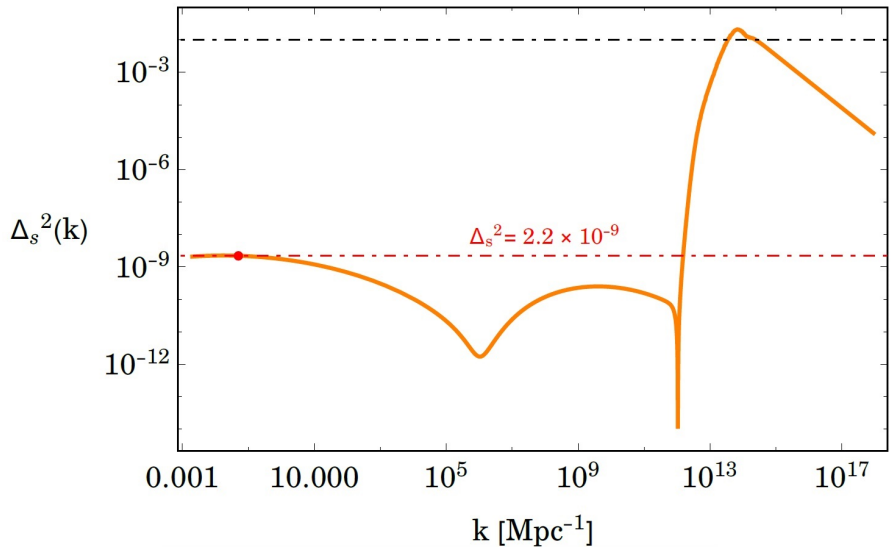

Figure 3.7: The exact power spectrum for the model [23], obtained for the set of values in (3.2.31).

while for the second set $\beta_1 \simeq 0.9$, $\beta_2 \simeq 0.16$ and $M_p/f = 1.7$ are used, letting the initial condition ϕ_0 remain still.
The results obtained for the two sets in [23] are the following

$$\begin{array}{c|c} n_s = 0.9672 & n_s = 0.9641 \\ \frac{\mathrm{d}n_s}{\mathrm{d}\ln k} = -0.0306 & \frac{\mathrm{d}n_s}{\mathrm{d}\ln k} = -0.0299 \\ r = 0.0079 & r = 0.0048 \end{array}$$

These sets are evaluated at pivot scale $N = 63.593$ the first and at $N = 54.015$ the second.

In this model the values for n_s seem to better fit the experimental expectations. Also the values for the tensor to scalar ratio r are in line with the observational constraints.
Let us now concentrate on the spectral running $\frac{\mathrm{d}n_s}{\mathrm{d}\ln k}$: its values lie outside the range provided by observations. This discrepancy can be attributed to the behaviour of the power spectrum at CMB scales, where in fact a bump can be observed, as we can seen in Figure 3.7. This significant curvature in the power spectrum on CMB scales is the responsible factor of the tension in the spectral running values.
We can hence state that the same tension arises in this model as in the others we have considered, but in this case this tension is hidden in the values of $\frac{\mathrm{d}n_s}{\mathrm{d}\ln k}$ rather than in n_s.

We stress that approximately the same results are obtained for all the models considered. For the fibre inflation model [14], [21] and [22] a tension occurs between the spectral index and the power spectrum amplitude, while for [23] it occurs between the spectral running and the power spectrum amplitude.
In an attempt to minimise this tension in the next chapter we will study a generalisation of the fibre potential considered above.

3.3 Modified Fibre Inflation

Since the model discussed above presents a tension between the calculated and the experimentally measured spectral index, we will study a different potential in an attempt to find a better agreement with the observations on CMB scales.
The potential considered thus far is fixed by the explicit geometrical embedding of fibre inflation [24], however to evaluate whether the low n_s can be avoided, we will allow ourselves the freedom to modify it to

$$V_{inf} = \frac{W_0^2}{\mathcal{V}^3}\left[\frac{-C_W}{\sqrt{\tau_{K3}}} + \frac{A_W}{\sqrt{\tau_{K3}} - B_W} + \left(\frac{-c_1\tau_{K3}^{p_1}}{1 + c_2\tau_{K3}^{p_2}}\right)\right]. \tag{3.3.1}$$

This potential has the same structure as that of equation (3.2.19). The only modification is regarding the field dependence in the third term: its powers p_1 and p_2 are no longer fixed to $(1, 3/2)$, but are taken to be free parameters. In general p_1 and p_2 must be positive with p_2 larger than p_1.

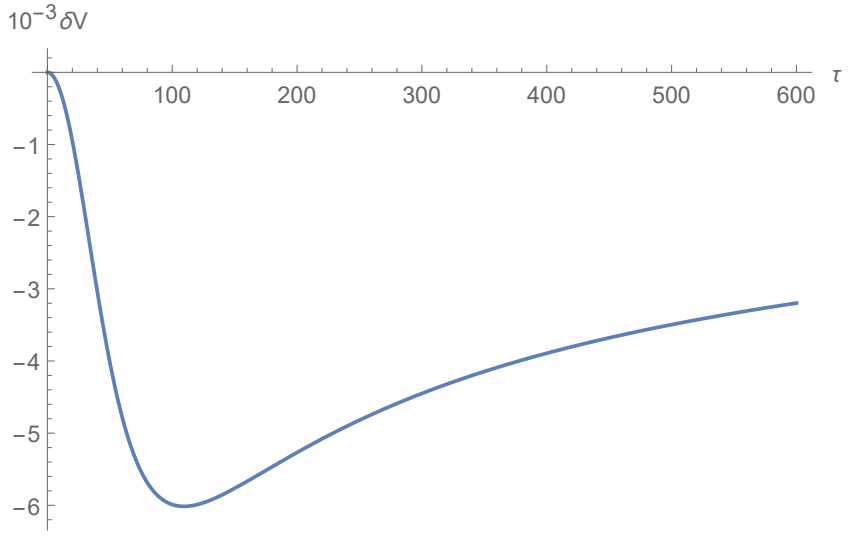

Figure 3.8: The figure shows the behaviour of δV for the set $\mathcal{S}_1$ in Table 3.3. For $c_2\tau^{p_2} \ll 1$, $\delta V \propto -\tau_{p_1} = -\tau^2$ and for $c_2\tau^{p_2} \gg 1$, $\delta V \propto -\tau_{p_1-p_2} = -\tau^{-1/2}$.

Let us analyse the new term we introduced $\delta V \equiv \left(\frac{-c_1\tau_{K3}^{p_1}}{1+c_2\tau_{K3}^{p_2}}\right)$. Two main behaviours can be noticed: for $c_2\tau^{p_2} \ll 1$ the denominator in δV takes a value close to unity and for this reason $\delta V \approx -c_1\tau^{p_1}$, while for $c_2\tau^{p_2} \gg 1$ δV reduces to $\delta V \approx -\frac{c_1}{c_2}\tau^{p_1-p_2}$. This behaviour is depicted in Figure 3.8 for the set $\mathcal{S}_1$ and is qualitatively similar to the original model [14].

Once we fixed the powers p_1 and p_2, the parameters c_1 and c_2 are tuned to obtain

the same behaviour for the scalar power spectrum on the CMB scales and the same amplification needed on the PBH scales we were searching for in the previous section. Numerical results are shown in Table 3.4.

	$\mathcal{S}_1$	$\mathcal{S}_2$	$\mathcal{S}_3$	$\mathcal{S}_4$
W_0	1.25	1.05	1.00	1.60
C_W	17/100	17/100	17/100	17/100
A_W	8/100	8/100	8/100	8/100
B_W	1	1	1	1
p_1	2	11/2	3/2	1/2
p_2	5/2	6	7/2	7/2
c_1	$2.515598 \cdot 10^{-6}$	$2.010074 \cdot 10^{-12}$	$1.008004 \cdot 10^{-5}$	$7.92944 \cdot 10^{-4}$
c_2	$3.19994 \cdot 10^{-5}$	$7.770105 \cdot 10^{-11}$	$7.99339 \cdot 10^{-8}$	$1.4820 \cdot 10^{-9}$
$\mathcal{V}$	450	450	450	600
$\langle \tau_{K3} \rangle$	10.6387	10.1452	10.6072	11.5045

Table 3.3: Numerical values for parameters in the potential (3.3.1).

	$\mathcal{S}_1$	$\mathcal{S}_2$	$\mathcal{S}_3$	$\mathcal{S}_4$
n_s	0.9462	0.9462	0.9514	0.9610
$P_k\|_{peak}$	0.0225765	0.015603	0.019925	0.0133112
Δ^{PBH}_{CMB}	35	35	35	35
r	0.00938821	0.00676202	0.00612086	0.0075268

Table 3.4: Observables n_s and P_k, which is evaluated in the peak at PBH scales, for the scalar power spectrum obtained through the sets presented in Table 3.3.

It is interesting to notice how the ultra slow-roll period behaves for different set of powers p_1 and p_2. In Figure 3.9 we can observe the variation of the length and position of the plateau depending on the different values of the powers p_1 and p_2.
Let us analyse the set $\mathcal{S}_2$: for this case the powers are both greater than the ones occurring in (3.3.1) and for this reason the potential presents a smaller ultra slow-roll region, the shortest of all our examples, see Figure 3.9.
The reduction of the duration of the ultra-slow roll periods can be better noticed comparing the behaviour of the slow-roll parameters ε and η for the set $\mathcal{P}_2$ in Figure 3.4 and $\mathcal{S}_2$ in Figure 3.10. In the first case the ultra slow-roll phase has a duration around 4 e-folds, while in the second around 2.5. In both cases $\Delta N^{PBH}_{CMB} = 35$.
Although the ultra-slow roll period becomes shorter as the powers become larger, for the set $\mathcal{S}_2$ it last a sufficiently long time such that we are able to obtain a scalar power spectrum that satisfies the normalization $\mathcal{O}(10^{-9})$ at CMB and the correct enhancement $\mathcal{O}(10^{-2})$ at PBH scales.

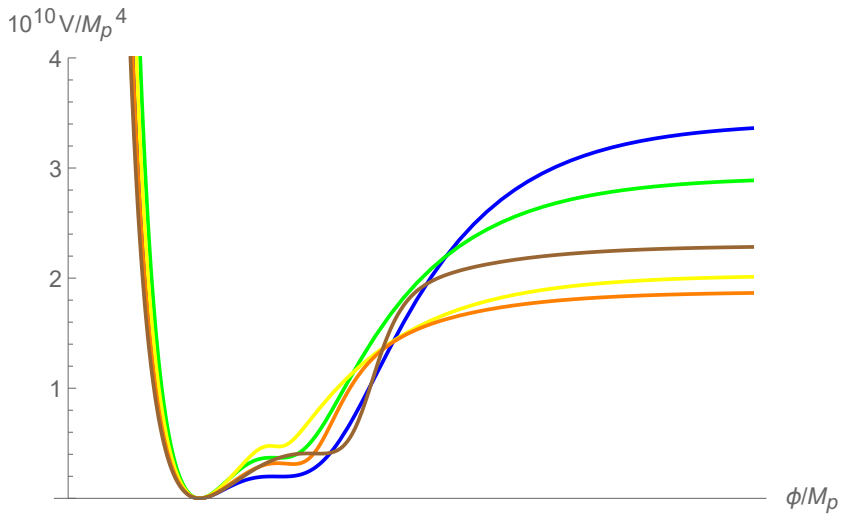

Figure 3.9: The figure shows the comparison between the potentials $\mathcal{S}_1$ (green line), $\mathcal{S}_2$ (yellow line), $\mathcal{S}_3$ (orange line) and $\mathcal{S}_4$ (brown line) in Table 3.3 and the set $\mathcal{P}_2$ (blue line) in Table 3.1. The potentials are shifted to the same minimum to allow the comparison.

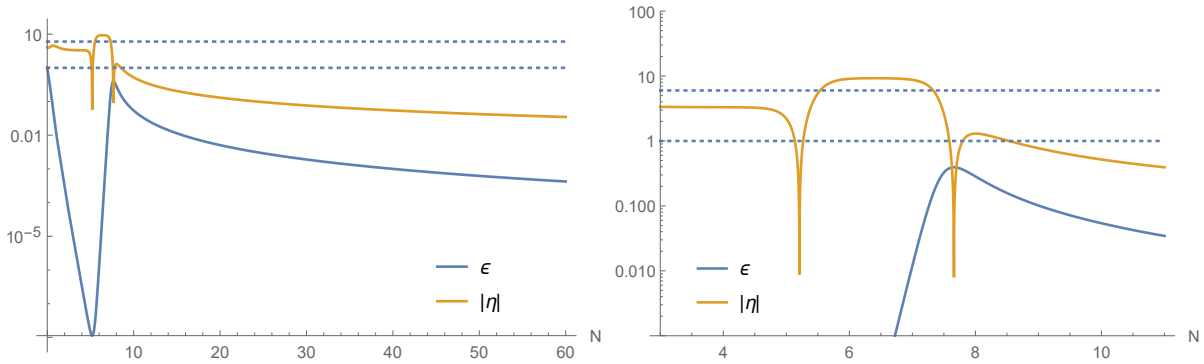

Figure 3.10: Left: The image shows the behaviour of the slow-roll parameters ε (blue line) and η (orange line) for $\mathcal{S}_2$ as functions of the e-folds number N in the complete domain of inflation. Right: from 3 to 11 e-folds. For $N > 7.5$ the system undergoes a slow-roll phase, for $4.5 < N < 7.5$ it enters the ultra slow-roll phase with η reaching almost 10, and finally for $N < 4.5$ the system faces a second slow-roll phase with $\eta = \mathcal{O}(1 - 10)$. At $N = 0$ inflation ends.

Regarding n_s, it tends to reach values that are closer to the experimental measurements (2.3.56) when the difference between the powers p_1 and p_2 becomes larger, as can be seen in Table 3.4.
In the sets $\mathcal{S}_1$ and $\mathcal{S}_2$, p_1 and p_2 differ for a factor of $1/2$, as in (3.2.19), and the corresponding spectral index is in fact similar to the ones found for all the parameter sets in

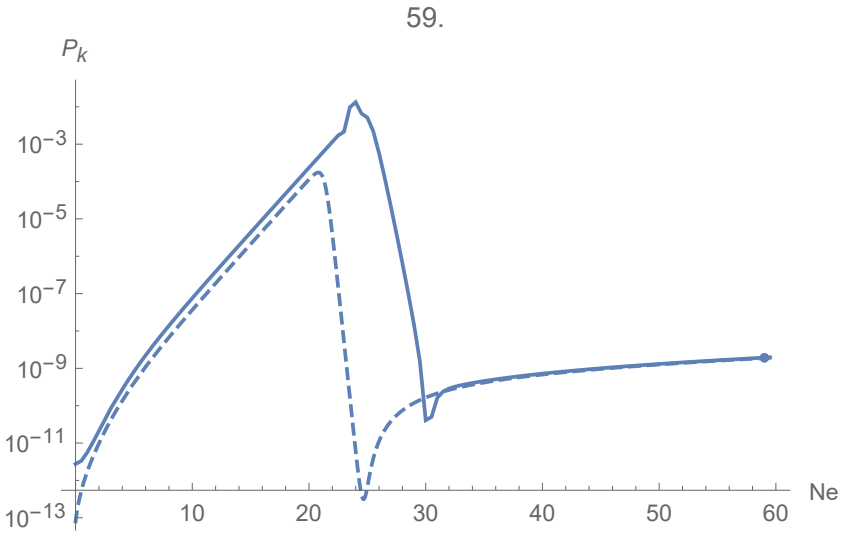

Figure 3.11: Scalar power spectrum evaluated at the end of inflation for the set $\mathcal{S}_4$. The continuous line has been obtained through the resolution of Mukhanov-Sasaki equation, while the dotted line represents the slow-roll approximation for the background. The e-folds number at which n_s is calculated is written in the upper part of the graph and it is represented in the graph by the circle.

the previous chapter.
In $\mathcal{S}_3$ and $\mathcal{S}_4$ the powers are chosen to be more different, in fact p_2 is larger than p_1 for a factor of 2 and 3 respectively. The former case presents a slightly better agreement with experimental values, while the latter perfectly fits the range in (2.3.56) and it reproduces the expected scalar power spectrum amplitude at the CMB scales and the right amplification at PBH scales, as can be seen in Figure 3.11.

We stress that, also for this model, the choices of the microphysical parameters are in line with expectations. The first two examples (set $\mathcal{S}_1$ and $\mathcal{S}_2$) lead to a spectral index similar to the one evaluated for the previous model, resulting 2 to 3 sigma redder than the current best fit. By increasing the difference in the values p_1 and p_2, an improvement in the spectral index can be observed: the most promising n_s can be seen for the set $\mathcal{S}_4$, which fits well enough the experimental measures. We further stress that for all sets both the scalar power spectrum amplitude at the CMB scales and its amplification at PBH scales are correct.

Conclusions

In this thesis we studied the possibility of PBHs contributing partially or totally to the present dark matter fraction and focused on satisfying the primordial power spectrum bounds both on CMB and PBH scale.

The first chapter provides a general introduction to standard cosmology, whose concepts are useful for the description of inflation. We introduced the main parameters as the scale factor a and the Hubble parameter H and analysed how historically the idea of inflation arose, starting from the problems Big Bang models presents and finding their solutions with the introduction of an inflationary period at early times.

In the second we mainly focused on the mathematical description of the inflationary phase. First, we studied the conditions required for inflation. We studied then how the background evolves using the Klein-Gordon equation starting from single-field models, with the homogeneous scalar field describing the inflaton.
Subsequently, we introduced perturbations and studied how they classically arise and evolve through the Mukhanov-Sasaki equation. Using the quantisation method on classical case, we obtained quantum perturbations, from which we could get a description for the power spectrum and its observables: the scalar amplitude P_k, the spectral index n_s and its running $\frac{\mathrm{d}n_s}{\mathrm{d}\ln k}$. Experimental measurements can provide us very precise constraints on the power spectrum amplitude at CMB scales and its spectral index and running at pivot scale $k = 0.05$ Mpc^{-1}.

The third chapter is dedicated to the analysis of PBHs formation and to the study of the power spectrum associated with the inflationary period. Furthermore we considered PBHs formation due to gravitational collapse of curvature perturbations following the Gaussian probability distribution and re-entering the horizon in a radiation dominated era. From observations we know that the power spectrum at CMB scales must be normalized at $\mathcal{O}(10^{-9})$ and, assuming a Gaussian probability distribution for primordial fluctuations and studying the total energy density of PBHs, we found the need to enhance the power spectrum to $\mathcal{O}(10^{-2})$ on PBH scales, in line with the estimates in the literature.

We considered fibre inflation models. In order to satisfy the enhancement required in the power spectrum at PBH scales and hence to allow the formation of PBHs, a further term to the fibre inflation potential must be added, which modifies the inflationary dynamics by giving rise to an ultra slow-roll phase induced by an extremely flat plateau-like region on PBH scales.
Through this analysis' mechanism we obtained the proper normalization in the power spectrum amplitude both at CMB and PBH scales, but a tension between the observations and the values of the spectral index obtained with this model arises. For this reason we proposed a mechanism in order to minimise this tension. Modifying the form of the additional term to fibre inflationary models and hence modifying the ultra slow-roll plateau form, we noticed that a better agreement with the observational values can be achieved. Therefore that tension can be explained as a consequence of the potential form we considered at first, while it can be avoided in models that provide a different plateau form.
We stress that the potential's form we considered generates PBHs at small scales via an efficient enhancement of the power spectrum due to a period of ultra slow-roll and provides parameters for the scalar power spectrum that are consistent with cosmological observations at CMB scales.

Appendix A

Code in Mathematica

The results and plots, if no source was given, discussed in the previous chapters are obtained computing a code in the software Mathematica.
Let us consider as example the calculation for the set $\mathcal{P}_2$.

First, we define the potential and its parameters.

```
W0 = 9.4690334348 ;
Cw = 4 / 100;
Aw = 2 / 100;
Bw = 1;
V = 1000;
Gw = 3.080548 * 10^-5 * V;
Rw = 7.071067 * 10^-4 * V;
τ = Exp[2 / Sqrt[3] * ϕ];
Vinf = W0^2 / V^3 ((-Cw) / Sqrt[τ] + Aw / (Sqrt[τ] - Bw) + τ / V (-Gw / (1 + Rw τ^(3/2) / V)));
```

This potential presents a minimum that we shift to zero, calculating the minima for the normalized field $\langle\phi\rangle$ and $\langle\tau_{K3}\rangle$ using the function **FindRoot**. In the code the minima for these fields go under the names ϕMin and τMin. The latter is the value contained in Table 3.1.

```
ϕMin = FindRoot[D[Vinf, ϕ] == 0, {ϕ, 1}]
τMin = τ /. ϕMin
Vtot = Vinf + Abs[Vinf /. ϕMin]
```

It is now useful to write V_{tot} in terms of the e-folds number N (Ne in the code).

```
VNe = Vtot /. {ϕ → ϕ[Ne]};
```

The next step is to solve the Friedmann equation (2.2.9) together with the Klein-Gordon equation (2.2.5), both expressed in terms of N. Let us evaluate the first and second derivatives taken with respect to the time t in terms of the derivatives taken with respect to N

$$\frac{\mathrm{d}}{\mathrm{d}t} = H\frac{\mathrm{d}}{\mathrm{d}N} \tag{A.0.1}$$

$$\frac{\mathrm{d}^2}{\mathrm{d}t^2} = H\frac{\mathrm{d}H}{\mathrm{d}N}\frac{\mathrm{d}}{\mathrm{d}N} + H^2\frac{\mathrm{d}^2}{\mathrm{d}N^2}, \tag{A.0.2}$$

and see how the equations become:

$$H\frac{\mathrm{d}H}{\mathrm{d}N}\frac{\mathrm{d}\phi}{\mathrm{d}N} + H^2\frac{\mathrm{d}^2\phi}{\mathrm{d}N^2} + 3H^2\frac{\mathrm{d}\phi}{\mathrm{d}N} = -\frac{\mathrm{d}V}{\mathrm{d}\phi} \tag{A.0.3}$$

$$\frac{\mathrm{d}H}{\mathrm{d}N} = -\frac{1}{2}H\left(\frac{\mathrm{d}\phi}{\mathrm{d}N}\right)^2. \tag{A.0.4}$$

The initial conditions used are $\phi_N = \frac{\mathrm{d}\phi}{\mathrm{d}N}(t=0) = 0$, $\phi_0 = \phi(t=0)$ fixed (in this case $\phi_0 = 10$) and $H_0 = H(t=0)$ calculated from equation (2.2.8) evaluated in $M_p = 1$ and $N = 0$

$$H(N) = \sqrt{\frac{1}{3}\left[\frac{1}{2}H^2\left(\frac{\mathrm{d}\phi}{\mathrm{d}N}\right)^2 + V(\phi)\right]} \tag{A.0.5}$$

$$H(0) = \sqrt{\frac{1}{3}V(\phi(0))}. \tag{A.0.6}$$

The differential equations are solved through the function **NDSolve** and inflation ends when the maximum value for N (we set $N = 10^5$) is reached or when ε reaches 1, stopping the calculation using the method **EventLocator**. In this way, H and ϕ are found.

```
ϕ0 = 10;
dϕ0 = 0;
```

```
solNe =
 NDSolve[{H[Ne] * H'[Ne] == -1/2 * H[Ne]^2 * ϕ'[Ne]^2,
   H[Ne] * H'[Ne] * ϕ'[Ne] + H[Ne]^2 * ϕ''[Ne] + 3 * H[Ne]^2 * ϕ'[Ne] == -D[VNe, ϕ[Ne]],
   H[0] == Sqrt[1/3 * (VNe /. (ϕ[Ne] → ϕ0))], ϕ[0] == ϕ0, ϕ'[0] == dϕ0}, {H, ϕ},
  {Ne, 0, 100000}, Method → {"EventLocator", "Event" → Abs[-D[H[Ne], Ne]/H[Ne]] - 1}]
HNe = H[Ne] /. solNe;
ϕNe = ϕ[Ne] /. solNe;
```

Using these solutions, we evaluated ε, η and the derivative of η (called η_N in the text and $D\eta$ in the code)

$$\varepsilon = -\frac{H_N}{H} = \frac{1}{2}\phi_N^2 \tag{A.0.7}$$

$$\eta = -\frac{2V_\phi}{H^2\phi_N} + 2\varepsilon - 6 \tag{A.0.8}$$

$$\eta_N = -2\left[\frac{V_{\phi\phi}}{H^2}\frac{V_\phi}{2H^2\phi_N}(4\varepsilon + \eta) - \varepsilon\eta\right], \tag{A.0.9}$$

where the subscripts N and ϕ represent the derivations with respect to the e-folds number and the field respectively.
To evaluate ε, η and η_N the equations (2.2.5) and (2.2.9) are used, in order to reduce the oscillation in plots, consequence of the way the software Mathematica works: the code solves derivatives numerically, causing oscillations in plots of functions containing them and the more we use them the more the oscillations become larger, since H and ϕ were already calculated as derivatives. To reduce this mechanism we use the equation of motion, limiting in this way the number of derivatives we use.

Now, the e-folds numbers where inflation ends and starts are set such that the total inflation has a duration of 60 e-foldings and the tensor to scalar ratio r is evaluated.

```
NeFIN = (H /. solNe)[[1, 1]][[1]][[2]]
NeIN = NeFIN - 60;

r = 16 ϵ /. (Ne → NeIN)
```

Let us define a and z. The variable n represents the number of points per e-folding we want to calculate (we set $n = 2$), while $N_{special}$ is a bias on N we used to decide the precision with whom we wanted to calculate that points.

```
a = Exp[Ne - NeIN];
z = √2 ϵ * a;
NSpecial = 55;
nPoints = 2;
```

We have to define some new variables in order to solve the Mukhanov-Sasaki equation. We write N_{HE}, the e-folds number at which the horizon exit occurs, N_{BD}, the e-folds where the Bunch-Davies conditions are evaluated, N_{END}, it represents 0.1 e-folding before inflation ends (otherwise the code could not finish at the right e-folding trying to reach for a larger value of N) and k, the scale we decide to evaluate the modes of the Mukhanov-Sasaki equation. To achieve that, we use **Table** to create vectors running along the index i_{Max}, which starts from the initial value of the inflation's e-folding N_{IN} and ends on N_{FIN}.

```
iMax = IntegerPart[NeFIN - NeIN] nPoints;
NeHE = Table[NeIN + i / nPoints, {i, 1, iMax}];
NeBD = Table[If[NeHE[[i]] > NSpecial, NeHE[[i]] - 10, NeHE[[i]] - 5], {i, 1, iMax}];
NeEnd = Table[NeFIN - 0.1, {i, 1, iMax}];
k = Table[a HNe /. {Ne → NeHE[[i]]}, {i, 1, iMax}];
```

We can evaluate the Mukhanov-Sasaki equation (2.3.9) for several scales using the Bunch-Davies condition (2.3.39). First, we have to write in terms of N the Mukhanov-Sasaki equation

$$v_{NN} + (1-\varepsilon)v_N + \left[\left(\frac{k}{aH}\right)^2 + \left(1+\frac{1}{2}\eta\right)\left(\varepsilon - \frac{\eta}{2} - 2\right) - \frac{\eta_N}{2}\right] v = 0, \tag{A.0.10}$$

and the Bunch-Davies conditions for v and v_N, where the phase is set to 1

$$v(N_{BD}) = \frac{1}{\sqrt{2k}} \tag{A.0.11}$$

$$v_N(N_{BD}) = -i\frac{\sqrt{k}}{\sqrt{2(aH)^2}}. \tag{A.0.12}$$

The Mukhanov-Sasaki equation is solved using a **For** loop running along i_{Max} in order to obtain several values of the mode for different k.

```
For[i = 1, i ≤ iMax, i++,
 tAux = AbsoluteTime[];
 MSsolAux[i] =
  NDSolve[{u''[Ne] + (1 - ϵ) u'[Ne] + (k[[i]]/(a HNe))^2 + (1 + 1/2 η) (ϵ - η/2 - 2) - Dη/2) u[Ne] == 0,
    u[NeBD[[i]]] == 1/Sqrt[2 k[[i]]],
    u'[NeBD[[i]]] == -I Sqrt[k[[i]]/Sqrt[2 (a HNe)^2 /. {Ne → NeBD[[i]]}]},
   u[Ne], {Ne, NeBD[[i]], NeEnd[[i]]}, MaxSteps → Infinity,
   Method → {"StiffnessSwitching", Method → {"ExplicitRungeKutta", Automatic}}][[1]];
 Print[NeHE[[i]] // N, "  ", AbsoluteTime[] - tAux]]
MSsol = Table[MSsolAux[i], {i, 1, iMax}];
```

Lastly, the scalar power spectrum (2.3.46) is evaluated through the solutions found from the Mukhanov-Sasaki equation in the previous step and saved in a **Table** called $MSsol$. A matrix called P_2 is created (also with **Table**) and used to store the values of the power spectrum with respect to the e-folding at which the modes exit the horizon.

```
P2 =
  Table[{NeFIN - NeHE[[i]],
    ((k[[i]]^3/(2 * Pi^2) * Abs[u[Ne]/z]^2) /. MSsol[[i]] /. Ne → NeEnd)[[1]][[1]][[1]]}, {i, 1, iMax}];


xpeak = Position[P2, Max[Transpose[P2][[2]]]][[1, 1]];
Npeak = P2[[xpeak]][[1]];
Ne35 = Npeak + 35;
x35 = Position[P2, Ne35][[1, 1]];

logP =
 Table[{Log[k[[i]]][[1]],
   (Log[k[[i]]^3/(2 * Pi^2) * Abs[u[Ne]/z]^2] /. MSsol[[i]] /. Ne → NeEnd)[[1]][[1]][[1]]},
  {i, x35 - 1, x35 + 1}]
angcoeff = LinearModelFit[logP, 1 + y, y];
nsMS = 1 + angcoeff[[1, 2, 2]]
```

The value of n_s is evaluated as in equation (2.3.48), fitting the logarithm of the power spectrum with respect to the logarithm of k around N_{35}, which is the e-folds number corresponding to the pivot scale exiting the horizon evaluated finding the maximum value

P_k reaches, called in the code N_{peak}, and adding $\Delta^{PBH}_{CMB} = 35$. For this procedure, another **Table**, called logP, is created to store the values of $\ln P_k$ and N_{HE}. To allow us to use the function **LinearModelFit** we have to include the package **"LinearRegression"**.

```
Needs["LinearRegression`"]
```

In the calculation of P_2, $N_{FIN} - N_{HE}$ is used instead of N_{HE} to obtain plots for inflation starting from $N = 60$ and ending at $N = 0$, otherwise it would have started at $N = N_{IN} \neq 60$ and ended in $N = N_{FIN} \neq 0$. The results remain the same, this change was only made to obtain plots that are easier to interpret.

As last step, the power spectrum amplitudes both at CMB and PBH scales are evaluated using the peak in the power spectrum corresponding to PBH scale and the first value of P_k we stored, corresponding to the value at CMB scale.

```
(*PBH scales*)
P2[[xpeak]][[2]]
(*CMB scales*)
P2[[1]][[2]]
```

Acknowledgements

I acknowledge my supervisor Dott. Francisco Gil Pedro for his great guidance and kindness.
A special thanks must be said to my buddies Michael and Mirko for sharing with me five years both of stressing moments and happy laughters.
Finally, my gratitude goes to my family. *A mio padre per tutto il supporto mostratomi negli anni. A mia madre per avere sempre creduto in me. A mio fratello per essere in grado di rendermi lievi anche i momenti più duri.*

Sara Zucchini

Bibliography

[1] P. Coles, F. Lucchin. *Cosmology-The Origin and Evolution of Cosmic Structure*, John Wiley & Sons, Ltd, 2002.

[2] E. W. Kolb, M. S. Turner. *The Early Universe*, Addison-Wesley Publishing Company, 1989.

[3] V. Mukhanov. *Physical Foundations of Cosmology*, Cambridge University Press, 2005.

[4] S. Weinberg. *Cosmology*, Oxford University Press, 2008.

[5] A. R. Liddle, D. H. Lyth. *Cosmological Inflation and Large-Scale Structure*, Cambridge University Press, 2000.

[6] R. D'Inverno. *Introducing Einstein's Relativity*, Clarendon Press, Oxford, 1992.

[7] S. Weinberg. *Gravitation and Cosmology: Principles and Applications of the General Theory of Relativity*, John Wiley & Sons, 1972.

[8] P. A. R. Ade *et al*. [Planck Collaboration]. *Planck 2015 results. XIII. Cosmological parameters*, Astron. Astrophys. 594 (2016) A13 doi: 10.1051/0004-6361/201525830 [arXiv:1502.01589v3 [astro-ph.CO]].

[9] D. Baumann *TASI Lectures on Inflation*, TASI (2009), [arXiv:0907.5424v2 [hep-th]].

[10] D. Baumann, L. McAllister *Inflation and String Theory*, Ann. Rev. Nucl. Part. Sci. 59 (2009) 67 doi:10.1146/annurev.nucl.010909.083524 [arXiv:0901.0265 [hep-th]].

[11] P. A. R. Ade *et al*. [Planck Collaboration]. *Planck 2015 results. XX. Constraints on inflation*, Astron. Astrophys. 594 (2016) A20 doi:10.1051/0004-6361/201525898 [arXiv:1502.02114 [astro-ph.CO]].

[12] N. Bartolo, V. De Luca, G. Franciolini, M. Peloso, A. Riotto. *The Primordial Black Hole Dark Matter - LISA Serendipity*, (2018) [arXiv:1810.12218v1 [astro-ph.CO]].

[13] B. Carr, F. Kuehnel, M. Sandstad. *Primordial Black Holes as Dark Matter*, Phys. Rev. D 94 (2016) no.8, 083504 doi:10.1103/PhysRevD.94.083504 [arXiv:1607.06077 [astro-ph.CO]].

[14] M. Cicoli, V. A. Diaz, and F. G. Pedro. *Primordial Black Holes from String Inflation*, (2017) doi:10.1088/1475-7516/2018/06/034 [[arXiv:1803.02837v2 [hep-th]].

[15] M. Sasaki, T. Suyama, T. Tanaka and S. Yokoyama. *Primordial Black Holes-Perspectives in Gravitational Wave Astronomy-*, Class. Quant. Grav. 35 (2018) no.6, 063001 doi:10.1088/1361-6382/aaa7b4 [arXiv:1801.05235 [astro-ph.CO]].

[16] G. Franciolini, A. Kehagias, S. Matarrese and A. Riotto. *Primordial Black Holes from Inflation and non-Gaussianity*, JCAP 1803 (2018) no.03, 016 doi:10.1088/1475-7516/2018/03/016 [arXiv:1801.09415 [astro-ph.CO]].

[17] M. Cicoli, C. P. Burgess, and F. Quevedo. *Fibre Inflation: Observable Gravity Waves from IIB String Compactifications*, JCAP 0903 (2009) 013 doi:10.1088/1475-7516/2009/03/013 [arXiv:0808.0691 [hep-th]].

[18] K. Becker, M. Becker, J. Schwarz. *String theory and M-theory-A modern introduction*, Cambridge University Press, 2007.

[19] K. Dimopoulos. *Ultra slow-roll inflation demystified*, (2017) doi:10.1016/j.physletb.2017.10.066 [arXiv:1707.05644v3 [hep-ph]]

[20] H. Motohashi, W. Hu. *Primordial Black Holes and Slow-Roll Violation*, Phys. Rev. D 96 (2017) no.6, 063503 doi:10.1103/PhysRevD.96.063503 [arXiv:1706.06784 [astro-ph.CO]].

[21] J. Garcia-Bellido, E. Ruiz Morales. *Primordial black holes from single field models of inflation*, Phys. Dark Univ. 18 (2017) 47 doi:10.1016/j.dark.2017.09.007 [arXiv:1702.03901 [astro-ph.CO]].

[22] G. Ballesteros, M. Taoso. *Primordial black hole dark matter from single field inflation*, Phys. Rev. D 97 (2018) no.2, 023501 doi:10.1103/PhysRevD.97.023501[arXiv:1709.05565 [hep-ph]].

[23] O. Özsoy, S. Parameswaran, G. Tasinato, I. Zavala. *Mechanisms for Primordial Black Hole Production in String Theory*, doi: 10.1088/1475-7516/2018/07/005 [arXiv:1803.07626v2 [hep-th]].

[24] M. Cicoli, D. Ciupke, V. A. Diaz, V. Guidetti, F. Muia and P. Shukla. *Chiral Global Embedding of Fibre Inflation Models*, JHEP 1711 (2017) 207 doi:10.1007/JHEP11(2017)207 [arXiv:1709.01518 [hep-th]].